CR-134681

ENVIRONMENTAL PROTECTION OF TITANIUM
ALLOYS AT HIGH TEMPERATURES

to

NATIONAL AERONAUTICS AND SPACE ADMINISTRATION

Technical Management
NASA-Lewis Research Center
Cleveland, Ohio

Contract NAS3-17761

July 18, 1974

by

E. C. Wright, R. A. Wood, and M. S. Seltzer

BATTELLE
Columbus Laboratories
505 King Avenue
Columbus, Ohio 43201

N74-34048

ENVIRONMENTAL PROTECTION OF TITANIUM ALLOYS AT HIGH TEMPERATURES

I. G. Wright, et al

Battelle, Columbus Laboratories
Columbus, Ohio

July 1974

N O T I C E

THIS DOCUMENT HAS BEEN REPRODUCED FROM THE
BEST COPY FURNISHED US BY THE SPONSORING
AGENCY. ALTHOUGH IT IS RECOGNIZED THAT CER-
TAIN PORTIONS ARE ILLEGIBLE, IT IS BEING RE-
LEASED IN THE INTEREST OF MAKING AVAILABLE
AS MUCH INFORMATION AS POSSIBLE.

1. Report No. NASA CR-134681	2. Government Accession No.	3. Recipient's Catalog No.
4. Title and Subtitle ENVIRONMENTAL PROTECTION OF TITANIUM ALLOYS AT HIGH TEMPERATURES		5. Report Date July , 1974
		6. Performing Organization Code
7. Author(s) I. G. Wright, R. A. Wood, and M. S. Seltzer		8. Performing Organization Report No.
		10. Work Unit No.
9. Performing Organization Name and Address Battelle - Columbus Laboratories 505 King Avenue Columbus, Ohio 43201		11. Contract or Grant No. NAS3-17761
		13. Type of Report and Period Covered Contractor Report
12. Sponsoring Agency Name and Address National Aeronautics and Space Administration Washington, D.C. 20546		
		14. Sponsoring Agency Code

15. Supplementary Notes

Project Manager, Mr. F. H. Harf, Materials and Structures Division, NASA-Lewis Research Center, Cleveland, Ohio 44135

16. Abstract

Evaluation of various concepts of protecting titanium alloys from oxygen contamination at 922 K (1200°F) and from hot-salt stress-corrosion at 755 K (900°F) indicates that oxygen-contamination resistance can be provided by a number of systems, but for hot-salt stress-corrosion resistance, factors such as coating integrity become very important. Titanium aluminides resist oxygen ingress at 922 K through the formation of alumina (on $TiAl_3$) or modified TiO_2 (on Ti_3Al, TiAl) scales. TiAl has some resistance to attack by hot salt, but has limited ductility. Ductile Ti-Ni and Ti-Nb-Cr-Al alloys provide only limited resistance to oxygen ingress, but are not greatly susceptible to hot-salt stress-corrosion cracking.

PRICES SUBJECT TO CHANGE

17. Key Words (Suggested by Author(s)) Protection of titanium alloys Oxidation Hot-salt stress corrosion Coatings Titanium alloys	18. Distribution Statement Unclassified - Unlimited
19. Security Classif. (of this report) Unclassified	20. Security Classif. (of this page) Unclassified

21. No. of Pages

NASA-C-168 (Rev. 6-71)

TABLE OF CONTENTS

LIST OF TABLES

ia

LIST OF FIGURES

LIST OF FIGURES (Continued)

LIST OF FIGURES (Continued)

id

FOREWORD

This report was prepared by the personnel of Battelle-Columbus, Columbus, Ohio, and describes original work performed under Contract NAS3-17761.

The contract was awarded to Battelle-Columbus by the NASA-Lewis Research Center. Technical monitoring was provided by the Project Manager, Mr. F. H. Harf of the Materials and Structures Division of the NASA-Lewis Research Center.

I. G. Wright, R. A. Wood, and M. S. Seltzer of Battelle-Columbus served as principal investigators.

The authors wish to acknowledge helpful discussions with Dr. H. R. Gray of the NASA-Lewis Research Center and with Dr. R. I. Jaffee of Battelle-Columbus during the course of this program. Thanks are also due to Battelle's Columbus Laboratories for sharing a portion of the cost of this study.

The contract was performed over the period June 25, 1973 to June 30, 1974.

SUMMARY

Various concepts of providing protection to titanium alloys from oxygen contamination at 922 K (1200°F) and from hot-salt stress-corrosion at 755 K (900°F) have been evaluated. It appears that resistance to oxygen contamination can be readily provided by a number of systems, but that for resistance to hot-salt stress-corrosion additional factors such as coating integrity assume great importance. Titanium aluminides can provide contamination protection, and Ti-35Al has some resistance to hot-salt cracking, but the limited ductility of these alloys reduces their potential as coatings. Oxygen-barrier coatings of Si, Al/Cr, Al/Cr/Mg, Al/TiAl₃ and TiAl on Ti-6Al-2Sn-4Zr-2Mo did not provide protection from hot-salt stress-corrosion attack at 755 K, and in some cases the susceptibility of the alloy to this form of attack was enhanced. A major failing of these coatings was the occurrence of cracks penetrating to the substrate, which apparently resulted from the poor ductility of the coatings.

Ductile alloys of Ti-Ni and Ti-Nb-Cr-Al exhibited limited resistance to oxygen contamination at 922 K, but were not further embrittled by exposure to hot salt in air at 755 K. These alloys might prove suitable coatings if the resistance to oxygen penetration can be improved.

Because of difficulties in obtaining suitable coatings, the effect of electrochemically-active elements in suppressing the titanium-salt corrosion reaction was not investigated, nor was the importance of the presence of a titanium-rich scale or corrosion product to the continuation of hot-salt corrosion reaction assessed.

ENVIRONMENTAL PROTECTION OF TITANIUM
ALLOYS AT HIGH TEMPERATURES

by

I. G. Wright, R. A. Wood, and M. S. Seltzer

1. INTRODUCTION

Under present conditions of use, titanium alloys are exposed to
operating temperatures and stresses below the threshold values for stress-
corrosion cracking, and so are creep-limited rather than stress-corrosion
limited.[1] At higher temperatures, titanium alloys are degraded by oxygen
contamination, and at higher stress levels, especially for extended exposure
times in a hot-salt environment, they are highly susceptible to stress-
corrosion cracking. Consequently any upgrading of titanium alloys for use
above the current use temperature of 700-755 K (800-900°F), and at higher
stress levels or for longer exposure times requires that some form of pro-
tection from or resistance to the environment be provided.

Oxygen contamination can probably be minimized by the use of
conventional oxidation-resistant barrier-layer coatings, but for stress-
corrosion-prone titanium alloys the integrity, ductility and fatigue-
resistance of present coatings are barely adequate. For instance, coatings
developed in a recent effort[2] showed good resistance to oxygen contamina-
tion but were only marginally effective against hot-salt stress-corrosion
attack, increasing the hot-salt stress-corrosion threshold stress (755 K
for 3.6×10^5 s/900°F for 100 h) from about 14 MN/m^2 (2 ksi) for uncoated
Ti-6Al-2Sn-4Zr-2Mo to only 28-69 MN/m^2 (4-10 ksi) for coated specimens.

Hot-salt stress-corrosion attack is thought to occur by a hydrogen
embrittlement process, in which the hydrogen is evolved from the hydration
of electrochemically-produced complex chlorides of titanium.[3] If electro-
chemical reactions do indeed play a major role in the hot-salt stress-
corrosion attack of these alloys, then the choice of an effective scheme of
protection from this form of attack is rendered difficult. Although the use
of a protective, barrier coating offers some advantages in terms of available
technology, in order to avoid catastrophic stress-corrosion in the event of
a coating failure (which need only be a small perforation), the coating must
be electrochemically less noble than the substrate in the hot-salt environ-
ment, and must not form easily-hydrolyzed halides.

Of the present generation of oxidation- and hot-corrosion-resistant
coatings for superalloys, of which the most resistant are the aluminide and
Co-Cr-Al-Y systems[4] and the Fe-Cr-Al-Y and Ni-Cr-Al-Si systems[5], all con-
tain elements which form halides which are hygroscopic or deliquescent, so
that a source of hydrogen will always be available near the titanium surface
at any coating failure. In addition, while most of the elements found in
these coatings exhibit less noble electrochemical behavior than titanium, and

so should corrode in preference to the substrate, it is doubtful that the electrochemical driving force would be sufficient to stifle the local electrochemical differences between different phases in the substrate and so prevent notch-formation. Elements which are strongly electropositive to titanium, such as magnesium[3], and probably zinc, cadmium, gallium, and indium, can apparently provide effective electrochemical protection.

In view of the dangerous situation resulting from even small flaws which would expose the substrate to the environment, an important additional requirement of a coating for titanium alloys is that it should possess good fatigue resistance.

The objectives of this program were to develop concepts and techniques for the protection of titanium alloys, in particular Ti-6Al-2Sn-4Zr-2Mo (Ti-6-2-4-2), against oxygen contamination at 922 K (1200°F) and hot-salt stress-corrosion at 755 K (900°F). The approach which has been taken to solve this problem was firstly to define alloy compositions in the Ti-Cr-Al-base system which would produce inherent protective (oxygen-barrier) oxide scales other than TiO_2. These compositions might then be applied to titanium alloys by pack diffusion to form solid solutions in the surface regions, or as separate-phase coatings. The effectiveness of these oxide films in preventing oxygen contamination was established by measurements of oxidation kinetics and microhardness changes and by electron-optical examination after isothermal exposure to air at 922 K (1200°F), under 1.33×10^4 N/m² (100 torr) pressure for 3.6×10^5 s (100 hours). Separate phase coatings on Ti-6-2-4-2, and other potential coating alloys, were subjected to the same test to allow other types of oxygen barrier layers to be evaluated. The protection afforded by these same modified alloys, coatings and coating alloys was also determined in a hot-salt stress-corrosion environment. Measurements of 0.2 percent offset yield strength, UTS and elongation to fracture, and detailed examination of sites of corrosive attack of sodium chloride coated coupons, after exposure for 3.6×10^5 s (100 hours) at 755 K (900°F) at various stress levels, were used to characterize the effectiveness of the protection.

In order to provide standards for the tests performed on the modified alloys and the coated alloys, the same tests were conducted on the uncoated, as-received Ti-6-2-4-2 alloy. The experimental program was divided into three major tasks; oxide mapping evaluation, hot-salt stress-corrosion evaluation, and oxygen contamination evaluation.

2. RESULTS AND DISCUSSION

A. Oxide Mapping Evaluation

(1) Ti-Cr-Al Alloys. The initial effort in this task was to prepare and oxidize a series of Ti-Cr-Al alloys to determine the alloy compositions required for the production of inherent, oxygen-barrier, protective scales. The alloys investigated are listed in Table 1.

TABLE 1. Ti-Cr-Al ALLOY COMPOSITIONS

Weight Percent			Atomic Percent		
Ti	Cr	Al	Ti	Cr	Al
37	--	63	25	--	75
65	--	35	50	--	50
84	--	16	75	--	25
77	8	15	69.4	6.6	24
70	15	15	63.4	12.5	24.1
67	25	8	64.3	22.1	13.6
100	--	--	100	--	--

Chemical analyses of the alloying constituents used in preparing the charges for arc melting are given in Table 2, which also contains data for the niobium used in a subsequent alloy series.

Charges of 0.140 kg total were prepared from these materials and melted in a water-cooled copper crucible in a tungsten electrode arc-melting furnace. Each charge was melted at least four times to ensure homogeneity, the individual melting time per cycle ranging from 264 to 285 s (4.4 to 4.75 minutes) at a maximum current of 1400 amps. The alloys were cast into finger ingots of approximate dimensions of 0.1 m long by 0.019 m diameter (4 by 0.75 inches). Weight changes during melting were minimal.

The ingots of the Ti-35Al* and Ti-16Al alloys were sliced into coupons of approximately 1.27 x 10^{-3} m (0.050 inch) thickness without diffi-culty, from which oxidation coupons 0.0127 by 0.0127 by 8.89 x 10^{-4} m (0.5 by 0.5 by 0.035 inch) were prepared. The Ti-63Al alloy and the chromium-

---

* Denotes weight percent for all subsequent alloy compositions.

TABLE 2. CHEMICAL ANALYSES OF ELEMENTS USED TO
PREPARE Ti-Cr-Al ALLOYS

Impurity Element Reported	Major Impurity Content, Percent			
	Titanium Sponge, Toho (Japan)	Aluminum, Alcoa (99.99% min.)	Chromium, Union Carbide Electrolytic LG (99.4% min.)	Niobium Wah Chang, E.B. Melted Grade 1 (99.7%)
H	0.009	--	0.048	--
C	0.019	--	0.005	0.0040
N	0.007	--	0.001	0.0042
O	0.07	--	0.55	0.0140
H_2O	0.009	--	--	--
Mg	--	0.001	<0.001	--
Si	<0.01	0.002	0.001	--
S	--	--	0.014	--
Cl	0.14	--	<0.003	--
Fe	0.04	0.002	0.011	--
Co	--	--	<0.009	--
Ni	--	--	0.001	--
Cu	--	0.002	0.0005	--
Zn	--	0.001	--	--
Mo	--	--	<0.001	--
Ta	--	--	--	0.1800
W	--	--	--	0.0400

containing alloys, however, began to crack during the slicing operation and so were annealed for 5.76×10^4 s (16 hours) at 1144 K (1600°F) then furnace cooled to 644 K (700°F) at 38K/h and finally air cooled to room temperature before further slicing. These slices were hand-ground to shape since the annealed alloys were still too brittle to allow machine grinding. A final surface finish of 600 grit was used on all the alloys; the effects of different degrees of surface finish were not investigated.

The coupons were degreased in ethyl alcohol before being oxidized in a continuously recording thermobalance equipped with a Cahn RG microbalance. Most oxidation data were obtained for isothermal exposures up to 3.6×10^5 s (100 h) at 922 K (1200°F) in 1.33×10^4 N/m^2 (100 torr) air, although some tests were run in 1.01×10^5 N/m^2 (760 torr) air and others under thermal cycling conditions. The oxidation kinetics of these alloys are shown in Figures 1a and 1b, and those for titanium, Ti-6-2-4-2 and for a Ti-55Ni alloy in Figure 1c, for comparison. The test details are given in Table 3. Most of the alloys oxidized in accordance with a parabolic rate law for some period (often in the initial stages) during the course of a 3.6×10^5 s (100 h) exposure, and the parabolic rate constants calculated for these periods are summarized in Table 4. All the Ti-Cr-Al-base alloys oxidized slower than 99.9% pure titanium and the Ti-6-2-4-2 alloy. In addition, the data in Table 3 indicate that a change in air pressure from 1.33×10^4 N/m^2 (100 torr) to 1.01×10^5 N/m^2 (760 torr) did not have any large effect on the oxidation kinetics of the Ti-16Al and Ti-35Al alloys, and that the Ti-16Al, Ti-35Al, and Ti-63Al alloys were resistant to thermal cycling from 922 to 423 K (1200 to 302°F).

The comparative values of the parabolic rate constants (Table 4) derived for the three titanium-aluminum intermetallics are slightly misleading for, as shown in Figure 1a, the Ti-35Al alloy gained the least weight in 3.6×10^5 s (100 h) exposures. These three titanium aluminides then, oxidize slowly at 922 K (1200°F) in 1.33×10^4 N/m^2 (100 torr) air, and although there is some overlap in the scatter bands for the kinetic data, the order is Ti-16Al > Ti-63Al > Ti-35Al.

The morphology of the scales produced on some of the alloys are illustrated in Figures 2 to 7. X-ray diffraction analyses of the scales produced, made from Debye-Scherrer photographs of scale scraped from the coupons using a tungsten carbide stylus, revealed only a few weak lines for α-Al_2O_3. The bulk scale on all the alloys (except Ti-63Al) was apparently TiO_2 (rutile) although it is possible that a thin, basal layer rich in αAl_2O_3 may have formed in places. In addition, the X-ray diffraction patterns contained several lines which could not be identified. These data are found in Table 5. Interestingly, Ignatov, et al[6] reported similar scale analyses on titanium-aluminum alloys containing up to 14 weight percent Al oxidized at 1073-1273 K (1472-1832°F) in air for up to 9×10^4 s (25 h), but considered the alumina to reside at the oxide/gas interface.
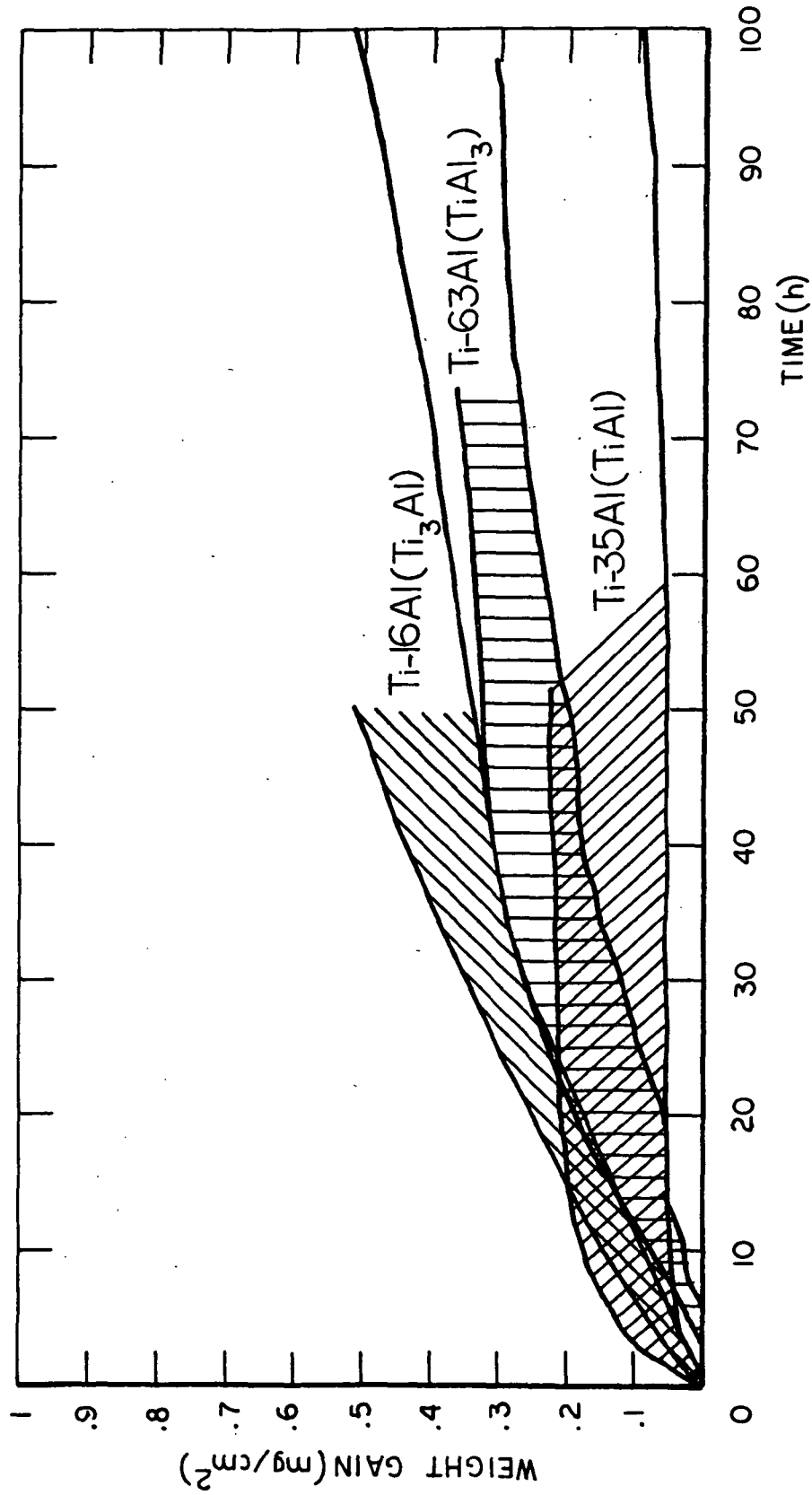
FIGURE 1a. ISOTHERMAL OXIDATION KINETICS OF TITANIUM ALUMINIDES AT 922K (1200°F) IN 1.33 x 10⁴ N/m² (100 TORR) AIR
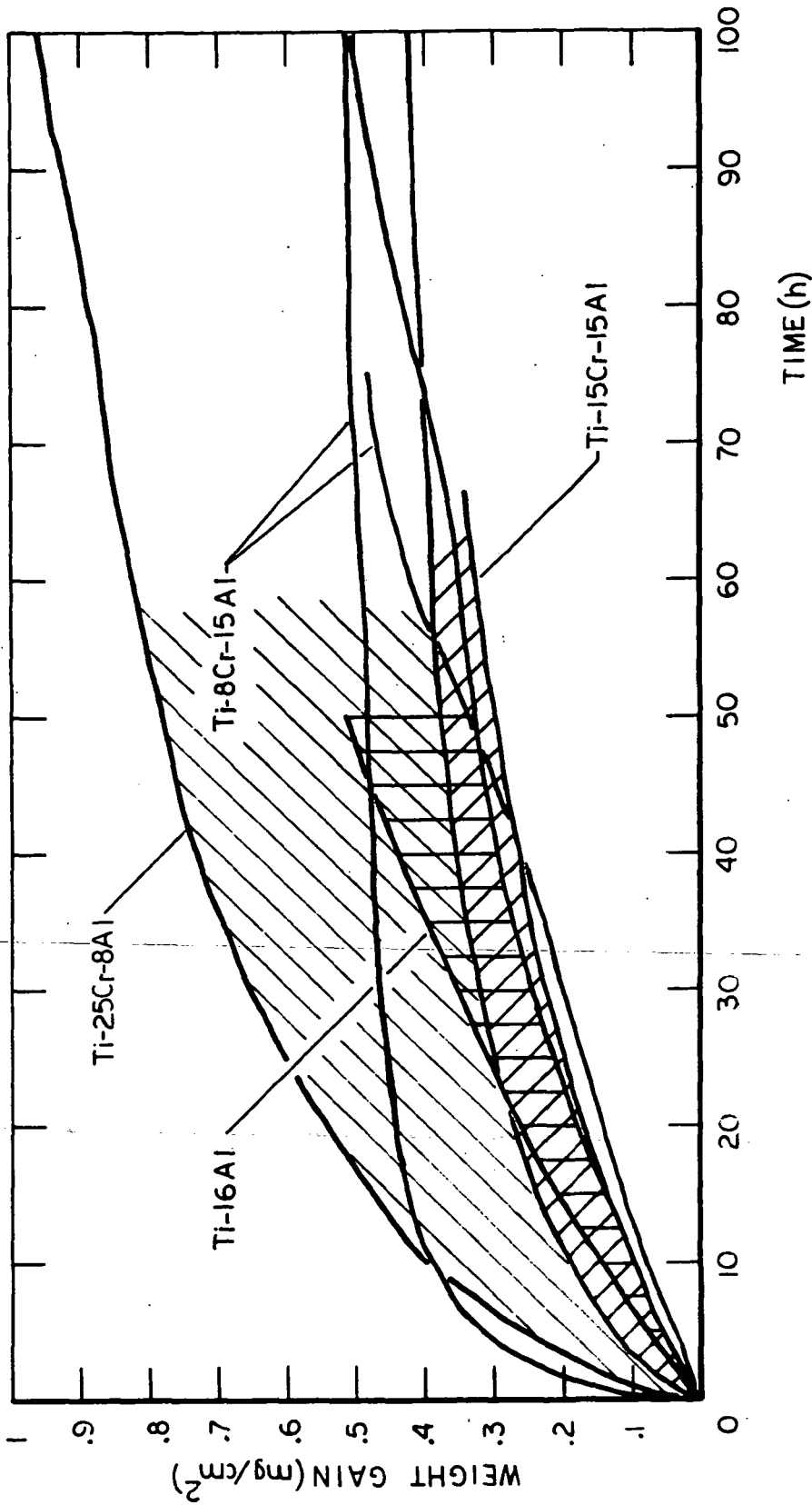
FIGURE 1: EFFECTS OF CHROMIUM ADDITIONS ON ISOTHERMAL OXIDATION KINETICS OF Ti$_3$Al AT 922K (1200°F) IN 1.33 x 10^4 N/m^2 (100 torr) AIR
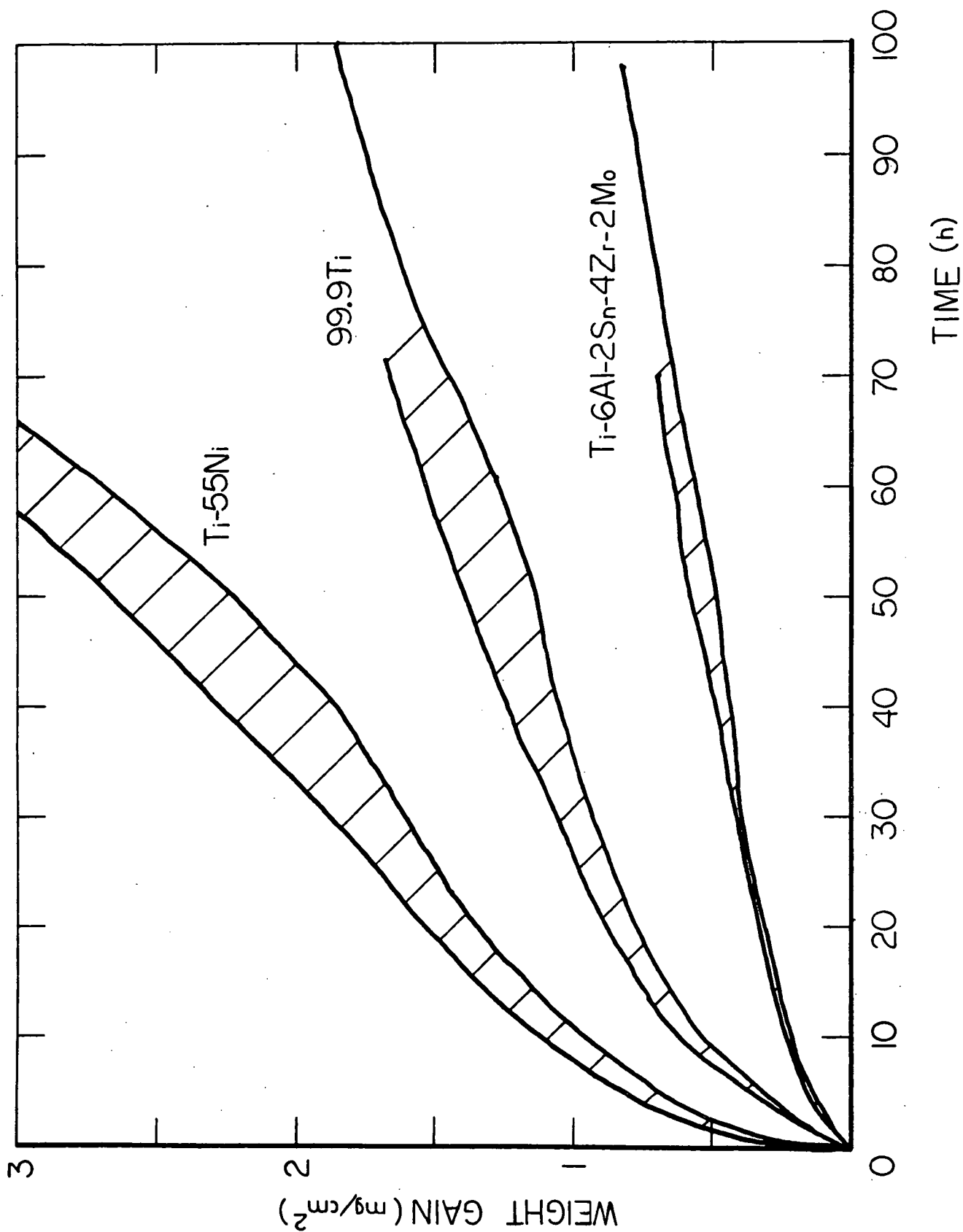
FIGURE 1c. OXIDATION KINETICS OF Ti, Ti-55Ni, and Ti-6Al-2Sn-4Zr-2Mo AT 922 K (1200°F) IN 1.33 × 10⁴ N/m² (100 torr) AIR

TABLE 3. DETAILS OF Ti-Cr-Al ALLOY OXIDATION TESTS AT 922 K (1200 °F) IN 1.33×10^4 N/m^2 (100 torr) AIR

Alloy	Specimen No.	Exposure Time s	Exposure Time h	Weight Gain (kg/m^2 x 10^2) Cahn	Weight Gain (kg/m^2 x 10^2) Check Weighing	Rate Index n*	Remarks
Ti	15	3.67×10^5	102	1.99	2.09	{1.4 (0-10 h) / 1.9 (10-100 h)	
	7	3.62×10^5	100.5	1.87	1.87	{0.9 (1-10 h) / 2.0 (10-70 h)	
	6	2.57×10^5	71.5	1.68	1.67		
Ti-16Al (Ti$_3$Al)	14	3.67×10^5	102	0.53	0.85	{1.0 (0-30 h) / 1.8 (30-100 h)	
	13	1.8×10^5	50	0.51	0.50	1.4	
	33	3.64×10^5	101	0.71	0.69	{2.0 (0-40 h) / 1.6 (40-101 h)	1.01×10^5 N/m^2
	36	2.07×10^5	57.5	0.23	0.25	--	Cyclic, 1.01×10^5 N/m^2
Ti-8Cr-15Al	24	3.64×10^5	101	0.53	0.46	{1.4 (0-4 h) / 7.5 (8-101 h)	
	27	2.7×10^5	75	0.48	0.48	1.1 (1-75 h)	
Ti-15Cr-15Al	12	3.65×10^5	101.5	0.44	0.43	{2.1 (0-25 h) / 4.7 (25-101 h)	
	8	2.39×10^5	66.5	0.36	0.50	1.6 (3-66 h)	
	35	3.64×10^5	101	--	0.26	--	1.01×10^5 N/m^2
	40	1.8×10^5	50	0.16	0.14	--	Cyclic, 1.01×10^5 N/m^2
Ti-25Cr-8Al	9	3.6×10^5	100	0.97	1.06	{2.1 (3-30 h) / 3.0 (30-100 h)	
	4	1.78×10^5	49.5	0.29	0.44	{2.2 (0-3 h) / 2.0 (7-49 h)	
	5	1.8×10^5	50	0.35	0.15	{1.0 (0-2 h) / 2.1 (2-50 h)	

TABLE 3. (CONTINUED)

Alloy	Specimen No.	Exposure Time (s)	Exposure Time (h)	Weight Gain ($kg/m^2 \times 10^2$) Cahn	Weight Gain ($kg/m^2 \times 10^2$) Check Weighing	Rate Index n^*	Remarks
Ti-35Al (TiAl)	2	4.32×10^5	120	0.15	0.14	$\begin{cases} 1.3 \ (0\text{-}4 \text{ h}) \\ 3.9 \ (4\text{-}120 \text{ h}) \end{cases}$	
	3	1.8×10^5	50	0.23	0.04	1.8 (1-15 h)	
	1	1.66×10^5	46	-0.02	0.04	--	
	30	2.56×10^5	71	0.10	0.10	--	Linde B Finish
	34	3.70×10^5	103	0.04	0.17	0.8 (0-103 h)	1.01×10^5 N/m²
	37	1.78×10^5	49.5	0.05	0.02	--	Cyclic, 1.01×10^5 N/m²
Ti-63Al (TiAl₃)	23	3.53×10^5	98	0.31	0.37	$\begin{cases} 0.8 \ (5\text{-}40 \text{ h}) \\ 1.5 \ (40\text{-}98 \text{ h}) \end{cases}$	
	28	2.63×10^5	73	0.36	0.49	~ 2 (0-73 h)	
	39	1.98×10^5	55	0.26	-0.1	--	Cyclic, 1.01×10^5 N/m²
Ti-6-2-4-2	21	3.53×10^5	98	0.83	0.79	1.8 (2-80 h)	
	22	2.34×10^5	65	0.67	0.67	1.9 (1-65 h)	
Ti-55Ni	18	2.88×10^5	80	3.82	3.60	$\begin{cases} 2.2 \ (0\text{-}40 \text{ h}) \\ 0.8 \ (40\text{-}80 \text{ h}) \end{cases}$	
	25	2.45×10^5	68	3.62	3.50	$\begin{cases} 2.3 \ (1\text{-}25 \text{ h}) \\ 1.0 \ (25\text{-}68 \text{ h}) \end{cases}$	
	26	8.64×10^4	24	1.51	1.47	2.0 (1-24 h)	

* From $w^n = kt$, where w = weight gain, n and k are constants, and t = time. For parabolic oxidation n = 2.0 and k = kp.

TABLE 4. SUMMARY OF OXIDATION KINETICS AT 922 K (1200°F)

	Parabolic Rate Constant (kg^2/m^4 s)	
Ti-Cr-Al Alloys	1.33×10^4 N/m^2 (100 torr)	1.01×10^5 N/m^2 (760 torr)
Ti-63Al	6.13×10^{-11}	
Ti-35Al	1.10×10^{-10}	
Ti-16Al	7.19×10^{-11}	1.13×10^{-10}
Ti-8Cr-15Al	--	
Ti-15Cr-15Al	8.00×10^{-4}	
Ti-25Cr-8Al	1.54×10^{-10}	
Ti	1.05×10^{-9}	
Nb-Ti-Cr-Al Alloys		
Nb-15Cr-15Al	(c)* 2.19×10^{-12}	
Nb-25Cr-8Al	(c)* 2.63×10^{-12}	
Nb-42Ti-9Cr-6.5Al	4.19×10^{-10}	
Nb-40Ti-9Cr-4Al	1.90×10^{-10}	
Nb-42Ti-4Cr-4Al	2.79×10^{-10}	
Other Alloys		
Ti-6Al-2Sn-4Zr-2Mo	1.86×10^{-10}	
Ti-55Ni	2.67×10^{-9}	

(c)* = cubic rate law, units kg^3/m^6 s.
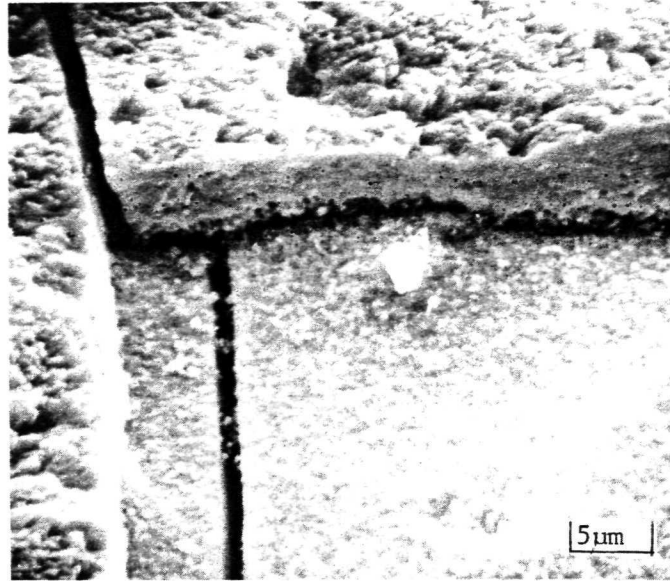
FIGURE 2a. 99.9% PURE TITANIUM OXIDIZED 3.67×10^5 s (102 h)
IN 1.33×10^4 N/m^2 (100 torr) AIR AT 922 K (1200 °F)

SEM Micrograph, 0.785 rad. tilt.
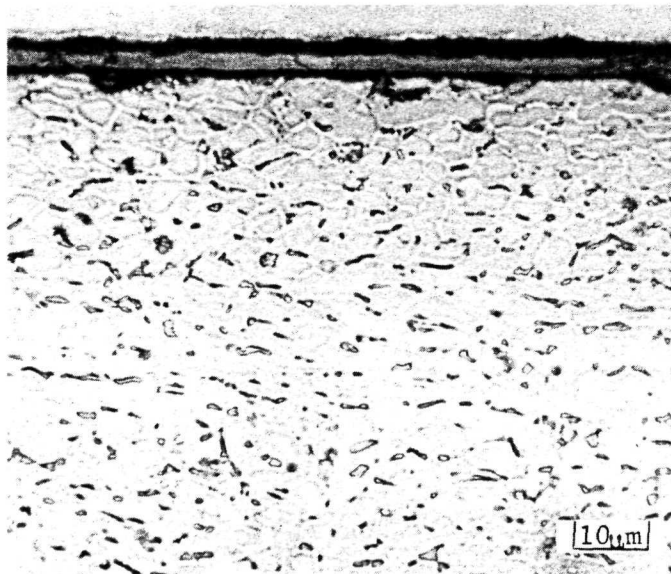
FIGURE 2b. Ti-6Al-2Sn-4Zr-2Mo OXIDIZED 3.53×10^5 s (98 h) IN
1.33×10^4 N/m^2 (100 torr) AIR AT 922 K (1200°F)
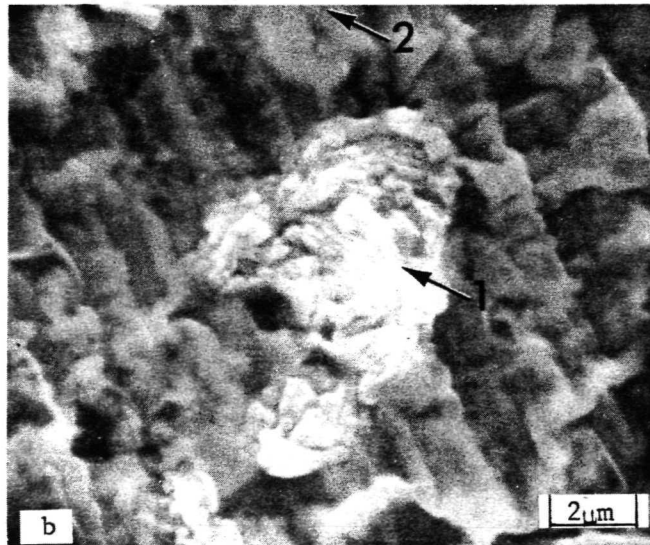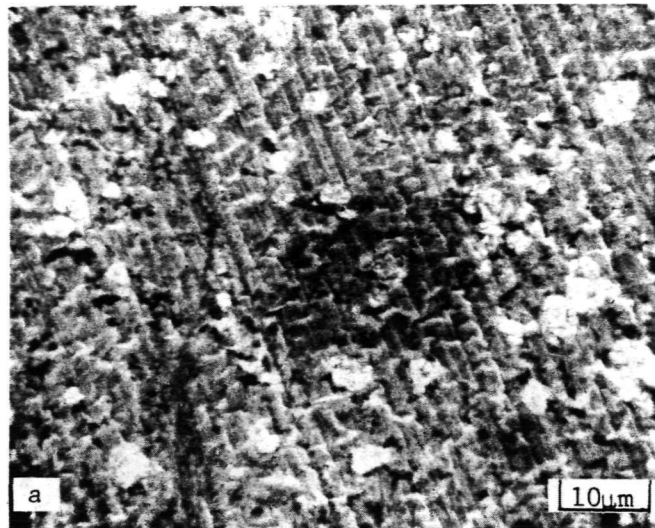
FIGURE 3. SCALE TOPOGRAPHY OF Ti-63Al ALLOY AFTER OXIDATION AT
922K (1200°F) FOR 3.53 x 10⁵ s (98 h) IN 1.33 x 10⁴
N/m² (100 torr) AIR

(a) General view of scale, showing wrinkled appearance, scratch
lines from original alloy surface, and white-appearing pro-
trusions. Dark area in center is area examined in detail
in SEM. 0.401 rad. tilt.

(b) Detail of (a). Protrusion No. 1 gave analysis: Ti:Al =
100:90, area 2 gave Ti:Al = 100:205. 0.227 rad. tilt.
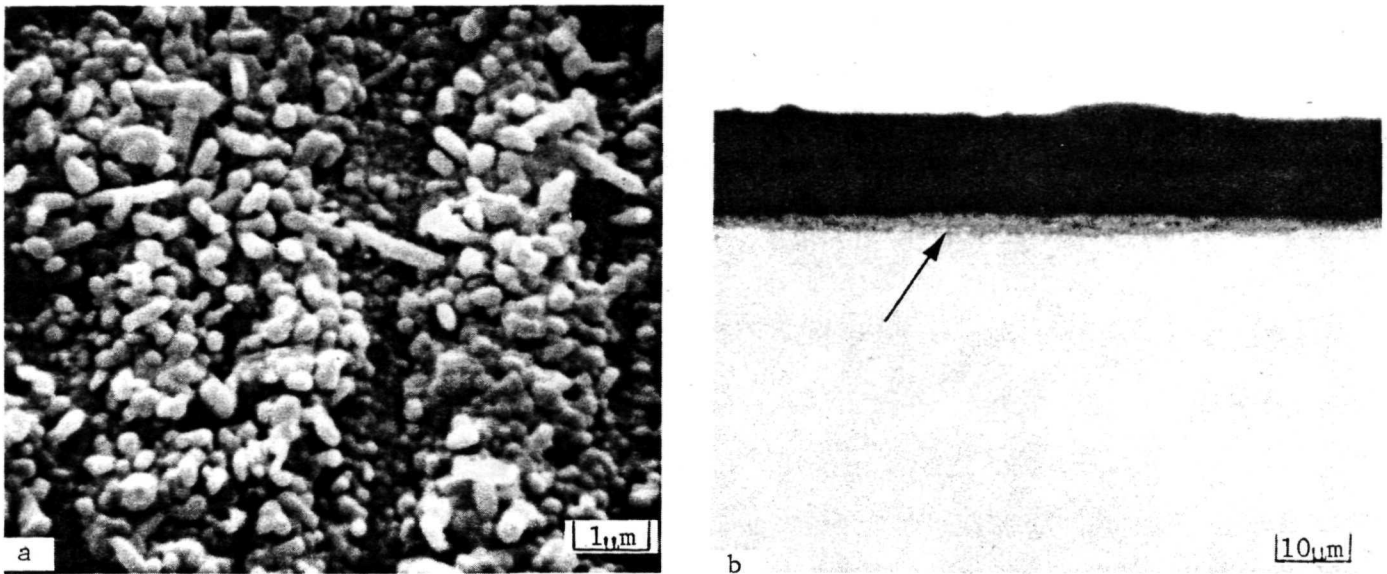
FIGURE 4.   SCALE FORMED ON Ti-35Al AFTER 4.32 x 10^5 s (120 h) OXIDATION
            AT 922 K (1200°F) IN 1.33 x 10^4 N/m^2 (100 **torr**) AIR

(a)   Scanning electron micrograph of outer surface of scale
      at 0.349 rad. tilt

(b)   Cross section
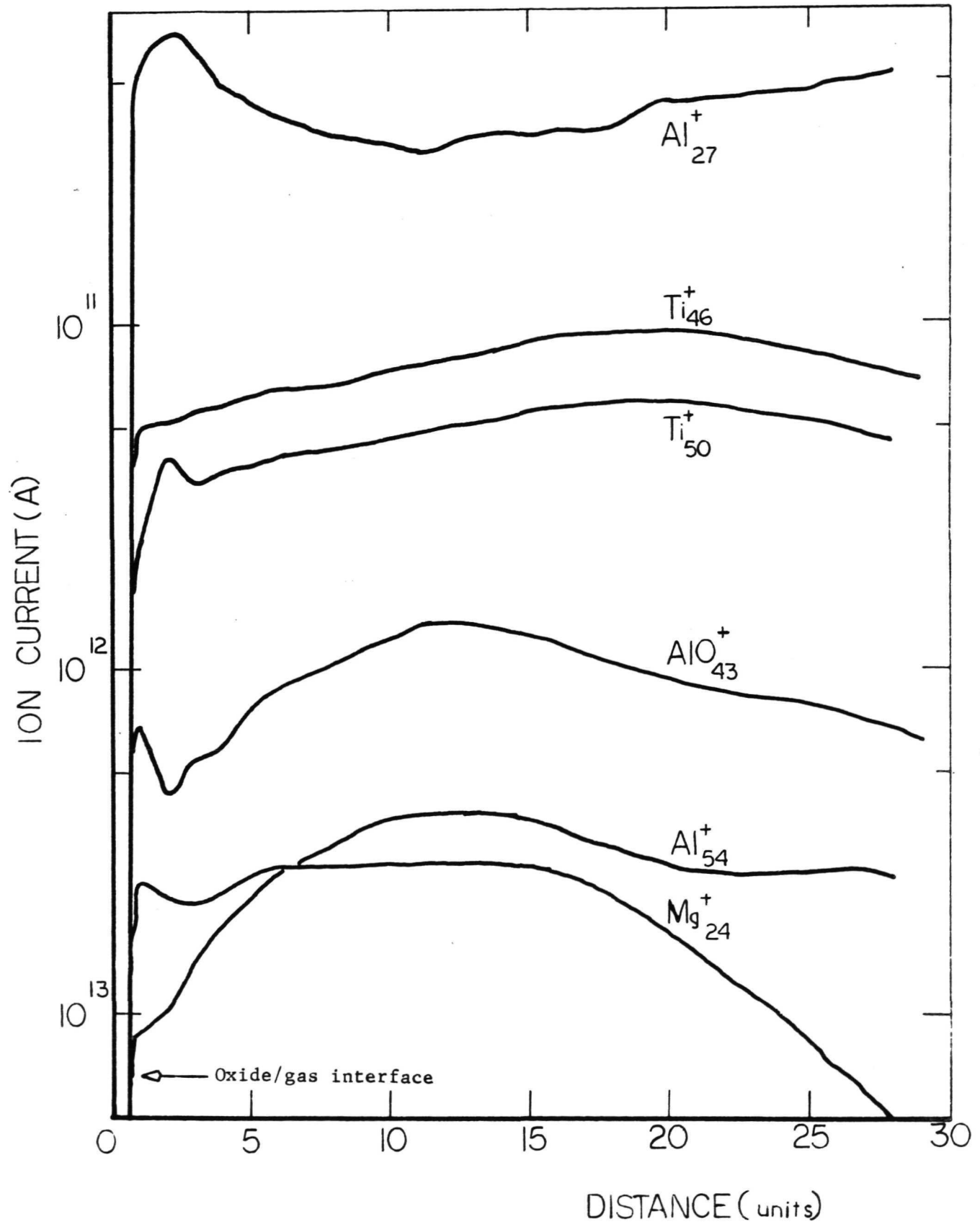
FIGURE 5. CONCENTRATION PROFILES THROUGH OXIDE SCALE
FORMED ON Ti-35Al AFTER 2.56 x 10^5 s (71 h)
IN 1.33 x 10^4 N/m^2 (100 torr) AIR AT
922 K (1200°F)
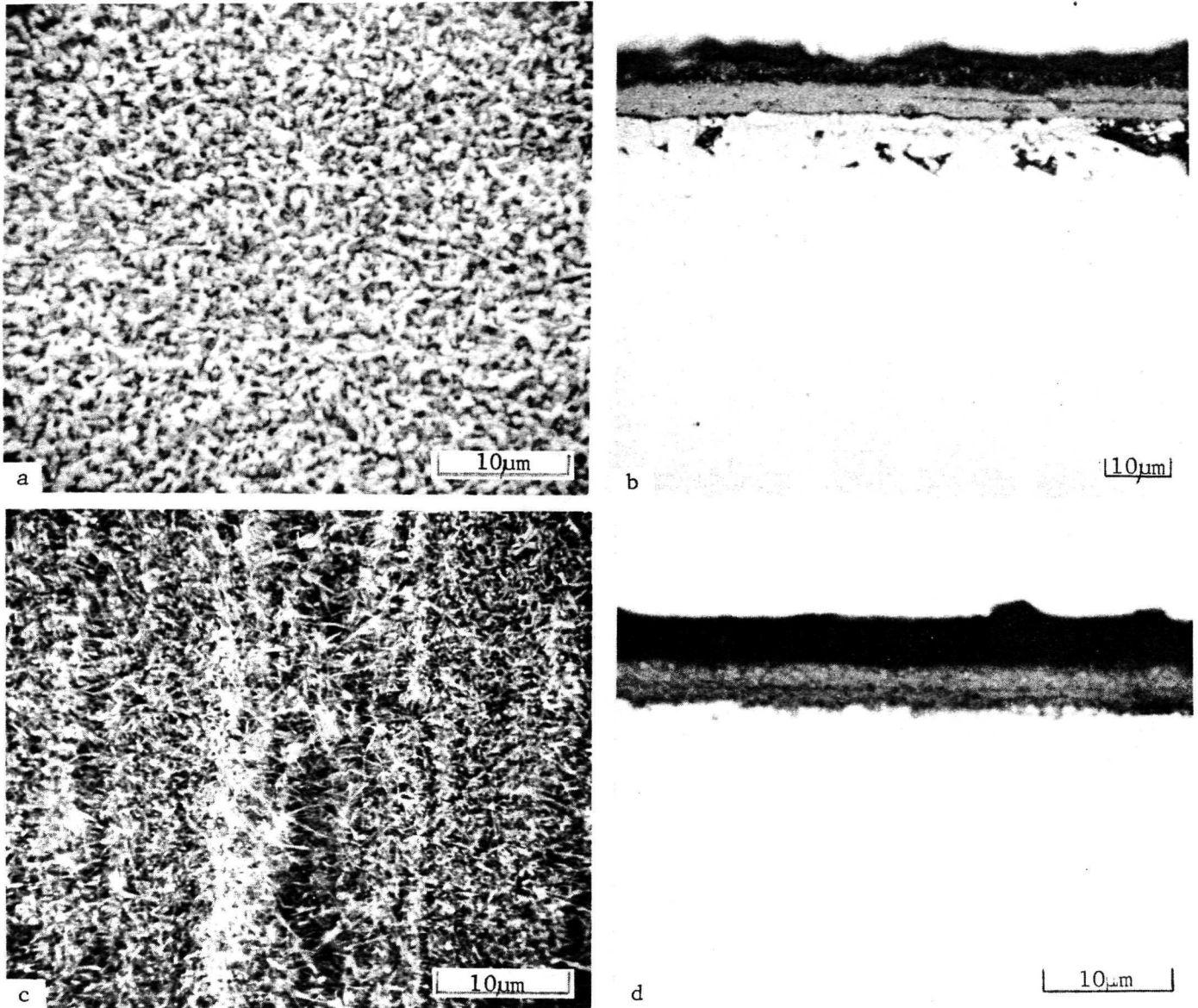
FIGURE 6. OXIDE SCALES FORMED ON Ti-Cr-Al ALLOYS AFTER OXIDATION AT
922 K (1200°F) IN 1.33 x 10^4 N/m^2 (100 torr) AIR

(a) Topography of scale on Ti-16Al alloy after 3.67 x 10^5 s
(102 h) (Specimen No. 14), back scattered electron (BSE)
image at 0.454 rad. tilt.
(b) Cross section of scale shown in (a).
(c) Topography of scale on Ti-15Cr-15Al alloy after 2.39 x
10^5 s (66.5 h) (Specimen No. 8). BSE image at 0.349 rad. tilt.
(d) Cross section of scale shown in (c).

a 5 μm

b 10 μm
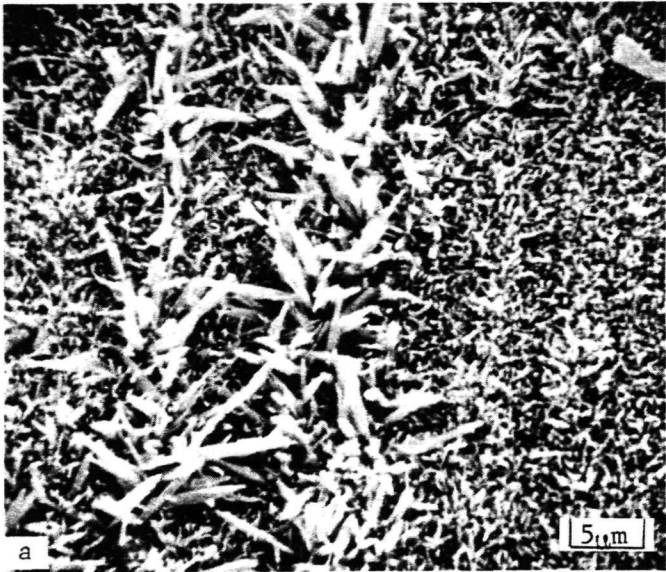
FIGURE 7.   SCALE FORMED ON Ti-25Cr-8Al AFTER 1.8×10^5 s (50 h)
OXIDATION AT 922 K (1200°F) IN 1.33×10^4 N/m^2 (100 torr) AIR

(a)   Scanning electron micrograph of outer scale surface
at 0.367 rad.

(b)   Cross section

TABLE 5. X-RAY DIFFRACTION DATA FOR SCALES FORMED ON Ti-Cr-Al ALLOYS

| STANDARD ASTM CARDS | | | | Ti-35% Al (No. 2) | | | Ti-15%Cr-15%Al (No. 8) | | | Ti-25%Cr-8%Al (No. 4) | | | Nb-40%Ti-9%Cr-4%Al (No. 10) | | |
TiO₂ (No. 21-1276) d	I/I₁	αAl₂O₃ (No. 10-173) d	I/I₁	d	I/I₁	SPECIES	d	I/I₁	SPECIES	d	I/I₁	SPECIES	d	I/I₁	SPECIES
													3.90	10	
		3.479	75				3.50	5	αAl₂O₃						
3.25	100			3.25	100	TiO₂	3.25	100	TiO₂	3.25	100	TiO₂	3.25	100	TiO₂
							3.05	5		3.08	5		3.03	10	TiO₂
										2.95	5				
				2.86	3								2.86	5	
										2.62	10		2.60	10	
		2.552	90	2.56	3	TiO₂	2.56	5							
2.48	50			2.48	30	TiO₂	2.48	80	TiO₂	2.48	80	TiO₂	2.48	90	TiO₂
		2.379	40	2.31	50	TiO₂	2.31	5	TiO₂	2.33	5	TiO₂	2.31	30	TiO₂
2.297	8									2.25	30				
2.188	25			2.18	30	TiO₂	2.18	60 } / 60	TiO₂	2.19	30	TiO₂	2.19	40	TiO₂
		2.165	41												
2.054	10	2.085	100	2.10	10	αAl₂O₃	2.10	5	αAl₂O₃	2.09	30	αAl₂O₃	2.07	5	αAl₂O₃
		1.964	2										1.93	5	
													1.88	5	
1.6874	60	1.740	45	1.74	5	αAl₂O₃				1.74	10	αAl₂O₃	1.75	5	αAl₂O₃
				1.685	30	TiO₂	1.68	40	TiO₂	1.69	50	TiO₂	1.69	90	TiO₂
1.624	20			1.62	5	TiO₂	1.62	10	TiO₂	1.62	20	TiO₂	1.63	40	TiO₂
		1.001	80										1.57	5	
		1.546	4												
		1.514	6												
1.497	10			1.48	3	TiO₂	1.48	10	TiO₂	1.45	5	TiO₂	1.48	30	TiO₂
1.45	10												1.455	30	TiO₂
1.42	2	1.404	50												
1.36	20	1.374	2	1.36	3	TiO₂				1.36	10	TiO₂	1.37	20	TiO₂
1.34	12	1.337	6							1.345	10	TiO₂	1.35	20	TiO₂
1.304	2	1.276	4												
1.244	4	1.239	16										1.245	5	TiO₂
		1.2343	8												
1.201	2	1.1898	8										1.175	5	TiO₂
1.170	5	1.1600	1												
1.148	2	1.1470	6												
		1.1382	2												
		1.1255	6										1.10	5	
		1.1246	4												
		1.0988	8												

Although the Ti-35Al alloy exhibited a faster parabolic rate constant in the early stages of oxidation (up to 5.4×10^4 s (15 h) than the Ti-16Al and Ti-63Al alloys, its rate of oxidation became slower than parabolic in the later stages. This is rather surprising because the Ti-63Al alloy formed an alumina scale, which is shown in Figure 3, whereas the Ti-35Al alloy formed a complex scale based on TiO_2 shown in Figure 4. The X-ray diffraction pattern obtained from a relatively large sample of this Al_2O_3 scale was very weak, indicating that the oxide might be largely amorphous to X-ray diffraction, but the observed lines were all accounted for by either α-Al_2O_3 (three major lines) or Ti-63Al (substrate). Analysis of the X-rays emitted from several of the larger, elongated oxide crystallites on the Ti-35Al alloy, using an Ortec Model 6200 analyzer attachment on a Cambridge Mk. II Stereoscan scanning electron microscope, gave compositions of Ti:Al of 100:36 (uncorrected values). Even though care was taken to analyze only large oxide crystallites fairly remote from the metal surface, these ratios are very close to the alloy composition and must be regarded with suspicion.

Careful electron-probe microanalysis of cross sections of the Ti-35Al alloy gave an approximate analysis for the thin scale of 20.7 Al, 31.5 Ti, aluminum being detected throughout the scale thickness, rather than forming an aluminum-rich basal layer. Although the scale on this alloy is very thin (1 to 2 μm), some noticeable change in aluminum signal would have been expected if an alumina layer were encountered by the electron microprobe.

Examination of the scale formed on a coupon of the Ti-35Al alloy oxidized with a Linde B surface finish (to provide a sharp metal/oxide interface) in a Cameca ion-probe also failed to detect any aluminum-rich layer. Instead, the scale appeared to have a relatively uniform composition throughout its thickness (Figure 5). It is therefore concluded that a complete layer of alumina is not formed on this alloy. In contrast, "large amounts" of alumina have been reportedly[7] detected in the scales formed on this alloy composition at 1073 to 1273 K (1472 to 1832°F) but no morphological details were given.

The kinetic curves in Figure 1b illustrate that additions of three levels of chromium to the Ti-16Al base exert little effect on the rate of oxidation but the scale morphologies on these four alloys are quite different, ranging from small, regular cyrstallites on the softest alloy, Ti-16Al, to very long, thin whiskers on the hardest alloy, Ti-15Cr-15Al (Figure 6). The scales are all basically TiO_2 modified with small amounts of aluminum and chromium, the weight ratios of Ti:Cr:Al ranging from 100:1:15 to 100:3:5 for the whiskers on the Ti-8Cr-15Al and Ti-15Cr-15Al alloys. No basal alumina layers were detected in these alloys.

For TiO_2, the Pilling-Bedworth ratio amounts to 1.77, which means that as grown, the scales are in compression. If it is assumed that the subsurface deformation in the softer, Ti-16Al alloy, resulted from stress relief of the scale, the whisker-like morphology of the outer scale on the harder Ti-15Cr-15Al alloy might be a direct result of the unrelieved stresses at the metal/oxide interface.

The scales formed on the Ti-25Cr-8Al alloy exhibited a dense array of needle- or blade-like outgrowths (Figure 7a), although in section the scale appeared relatively uniform (Figure 7b). In situ analysis of the larger blades gave uncorrected compositions of 100:17:5:4:1, Ti:Al:Cr:V:Mn, while careful siting of the X-ray source in the tips of the large blades gave 100:7:9, Ti:Al:Cr with a trace of silicon. Electron-probe microanalysis of the thin surface scale on the Ti-25Cr-8Al alloy gave compositions ranging from 34.5 Ti, 5.8 Cr, and 5.8 Al at the outer edge, to 45.4 Ti, 18.2 Cr, and 3.9 Al at the inner edge, although it must be remembered that some smearing out of concentration profiles is expected from overlap of the X-ray source with the substrate during analysis of thin scales. The alloy surface beneath this scale was apparently enriched in titanium by 4 weight percent, and depleted in Cr and Al, each by 2 weight percent, over a distance of approximately 7 μm.

An assessment of the capability of the Ti-55Ni alloy of providing protection against oxygen contamination when used as a coating was made by exposing it under the conditions of this test. The oxidation kinetics of this alloy are shown in Figure 1c and Tables 3 and 4, and the scale morphology is shown in Figure 8. The scale formed by this alloy comprised an outer layer of apparently TiO_2, with an extensive subscale of nonuniform thickness composed of a zone of unoxidized alloy enriched in nickel (white areas in subscale in Figure 8) containing brown-colored titanium oxide (dark areas in subscale in Figure 8). The parabolic kinetics observed for the first 8.64×10^4 - 1.44×10^5 s (24-40 h) of exposure appear to be related to the formation of the external scale and the titanium-depleted surface zone, while the increased oxidation rate observed after about 1.4×10^5 s (40 h) corresponds to the appearance of titanium oxide in this zone.
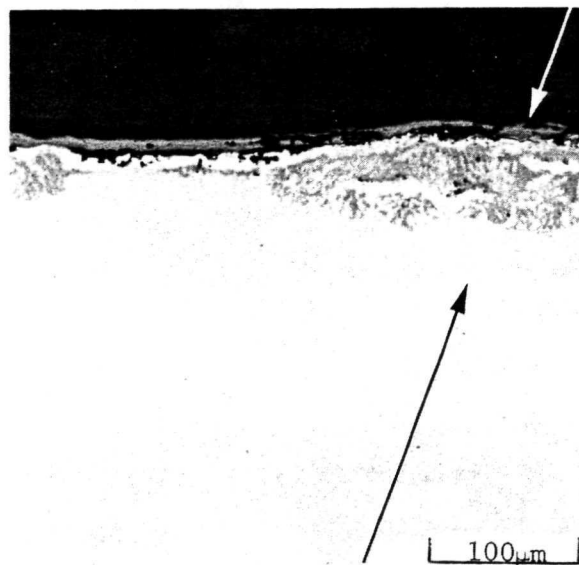
FIGURE 8. CROSS SECTION OF Ti-55Ni ALLOY OXIDIZED 2.88×10^5 s (80 h) AT 922 K (1200°F) IN 1.33×10^4 N/m² (100 torr) AIR

Arrows indicate path of electron microprobe step scan.

The main conclusion to be drawn from these results is that the Ti-Cr-Al alloys studied, with the exception of the brittle Ti-63Al alloy, do not form alumina-rich outer scales. The fact that the Ti-35Al and Ti-15Cr-15Al alloys in particular oxidized at a slower rate than unalloyed titanium is, however, of considerable interest, but the search for a protective, replacement scale in this alloy system does not look promising. For this reason, consideration was given to the formation of alumina-rich scales on niobium-base alloys.

(2) **Ti-Nb-Cr-Al Alloys.** The affinity for oxygen of aluminum is greater than that of niobium, while chromium has about the same affinity as niobium (where Nb_2O_5 is formed), so that it should be possible to form Al_2O_3 (and Cr_2O_3) scales on Nb-Cr-Al alloys by suitable alloying additions. Single additions to niobium of chromium above about 20 weight percent[8], and of up to 15 weight percent aluminum to Nb-25Ti alloys[9] apparently exert beneficial effects on the oxidation resistance, and ternary alloys Nb-28Ti-6Cr[10], Nb-68.3Ti-33.3Al[3] and the more complex alloys Nb-19Cr-10Al-15Co[11] and Nb-10Cr-10Al-15Ni-4W-2Ce[11] are apparently reasonably oxidation resistant. In addition, niobium and titanium have extensive solid solubility, so that Nb-Cr-Al coatings should be quite compatible with titanium alloys.

The alloy compositions studied are listed in Table 6. The alloys were arc melted and cast into finger ingots, with the exception of the T-166 alloy, which was available in sheet form. The ternary alloys, especially the Nb-10Cr-10Al alloy, proved extremely brittle, so that much effort was required to prepare suitable coupons for oxidation testing. The best of these contained a network of fine craze cracks.

TABLE 6. Ti-Nb-Cr-Al-BASE ALLOY COMPOSITIONS

Weight Percent				Atomic Percent				
Ti	Nb	Cr	Al	Ti	Nb	Cr	Al	Remarks
--	70	15	15	--	47.2	18.1	34.8	Brittle
--	80	10	10	--	60.5	13.5	26.0	Very brittle
--	67	25	8	--	48.1	32.1	19.8	Brittle
42	42.5	9	6.5	50.1	26.2	9.9	13.8	--
40	47	9	4	50.2	30.4	10.4	8.9	Solar J composition[12]
42	50	4	4	53.5	32.8	4.7	9.0	T-166[13]

Two alloys of this series, Nb-15Cr-15Al and Nb-25Cr-8Al, formed very thin, tenacious oxide films upon oxidation at 922 K in 1.33×10^4 N/m^2 air and, after considerable difficulties, the scale on the former alloy was identified as γ-alumina.

This scale is shown in Figure 9, to be relatively smooth, but was broken along either cracks or grain boundaries in the alloy surface and, from what could be seen of the metal oxide interface, the fit of the oxide to the alloys was good. Abrasion lines from the specimen surface finish were still visible on the surface of the scale (Figure 9a, b), and some fine cracking (Figure 9b) was also observed. Spot analysis of the region indicated in Figure 9a by arrow 1, using an X-ray detector attached to the SEM, gave weight ratios of Nb:Cr:Al of 100:70:36, compared to 100:20:40 for the exposed alloy indicated by arrow 2, and 100:22:22 expected from the nominal alloy composition. Clearly the X-ray source is detecting an aluminum and chromium enrichment in location 1, and an aluminum enrichment in location 2. Figure 9c shows the uniformity of the scale in cross section, and the group of electron microprobe images of this same area, in Figures 9d to g, show that the scale is aluminum-rich, and contains little niobium or chromium. This is confirmed by the line-scan shown in Figure 10, which also indicates that the bright areas in the alloy in Figure 9b correspond to a mole ratio of Nb:Cr:Al of 1:1:1, and the dark areas to Nb:Cr:Al of 6:1:3.

Representative kinetic curves for the Nb-Cr-Al alloys are shown in Figure 11, and details of the tests are given in Table 7. The form of these curves is similar to that expected of unalloyed niobium -- an initial period of protective oxidation (in this case according to a cubic rate law; see Table 4), followed by breakaway, rapid oxidation. In the case of unalloyed niobium the breakaway results from the formation of a porous, nonprotective Nb_2O_5 scale.

Careful examination of the scales formed on the Nb-Cr-Al alloys indicated that the breakaway kinetics observed were caused by oxidation proceeding down cracks in the alloy coupons rather than by the production of thick, nonprotective scales. In fact, after oxidation, parts of these coupons disintegrated into fine pieces of alloy, each piece being covered with a thin oxide layer. It is also possible that the actual oxidation rates may have been considerably lower than those measured, since the surface area of alloy exposed in cracks was not taken into account. The main body of the remaining coupon was covered with a thin oxide scale up to the edge at which disintegration occurred, with no signs of excessive porous scale formation. Figure 12a shows a surface view of the thin scale formed on the Nb-25Cr-8Al alloy. The alloy phases are visible, probably seen through the thin scale, and electron-probe analyses at points A and B probably represent the compositions of these phases rather than of the scale. Figure 12b is an oblique view of the alloy surface adjacent to the point of specimen disintegration (foreground), and shows some platelets of apparently similar composition to the alloy at B (C in Figure 12c) growing out of the alloy surface. Smaller mounds of oxide which grew in random patches, apparently over the dark-appearing alloy phase, also gave niobium-rich analyses (D in Figure 12c, E in Figure 12d), but these patches covered only a small part of the surface.
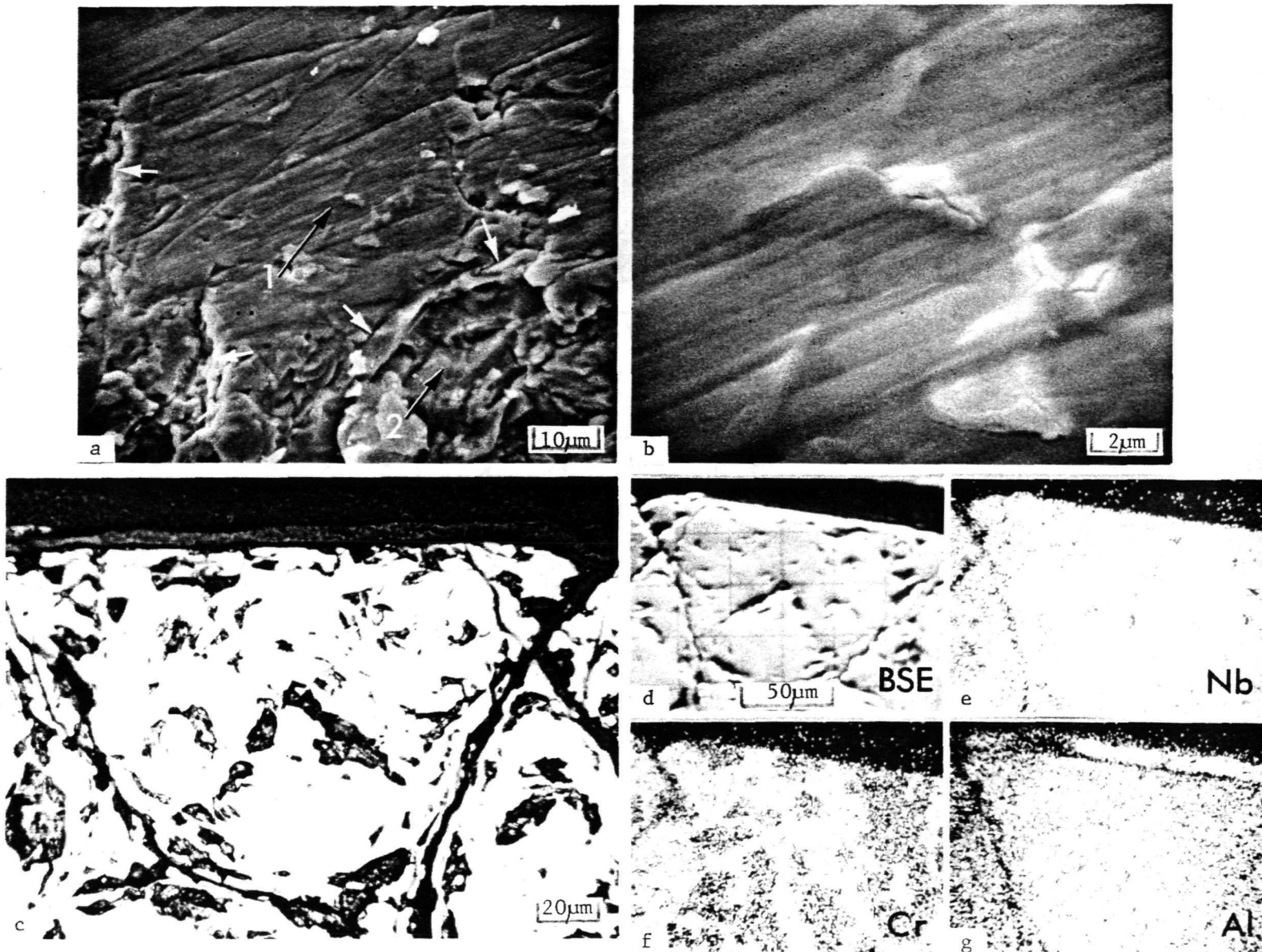
FIGURE 9. Nb-15Cr-15Al AFTER OXIDATION FOR 1.15×10^5 s (32 h) AT
922 K (1200°F) IN 1.33×10^4 N/m^2 (100 torr) AIR

(a) Topography of scale. White arrows indicate what is apparently alloy/
oxide interface at a fissure in the scale. Area 2 is exposed alloy
surface (Specimen No. 17). Backscattered electron (BSE) image at
0.436 rad. tilt.

(b) Enlarged view of scale surface from center of (a) (arrow No. 1). BSE
image at 0.436 rad. tilt.

(c) Cross section of alloy showing internal cracking.

(d) BSE image (mirror image) of same area as (c).

(e) to (g) X-ray images from area shown in (d), respectively for Nb Kα radiation,
Cr Kα, and Al Kα, showing the aluminum-rich scale.
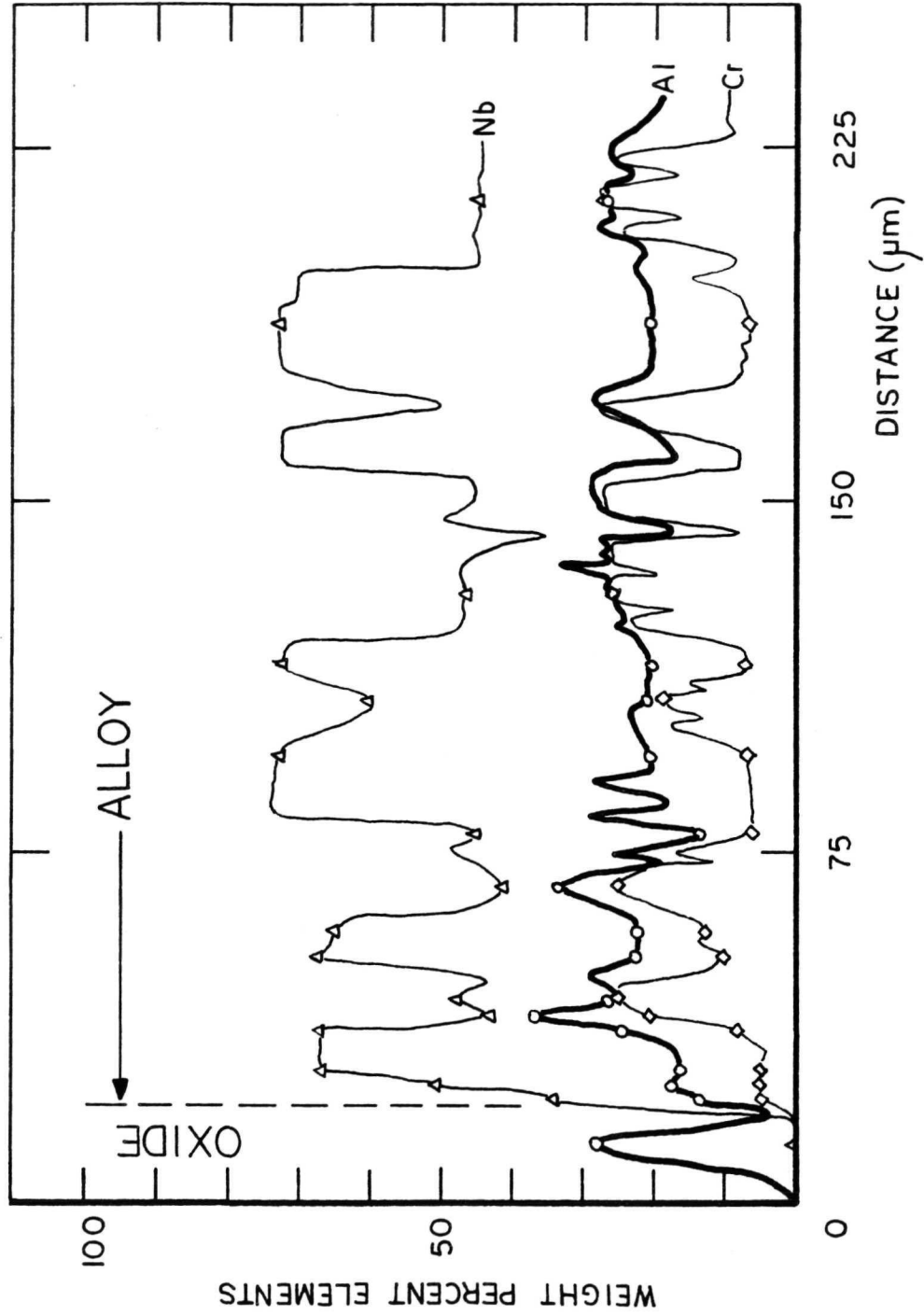
FIGURE 10. ELECTRON-PROBE CONCENTRATION PROFILE THROUGH CROSS SECTION OF Nb-15Cr-15Al ALLOY OXIDIZED FOR 1.15×10^5 s (32h) AT 922K (1200°F) IN 1.35×10^4 N/m^2 (100 torr) AIR
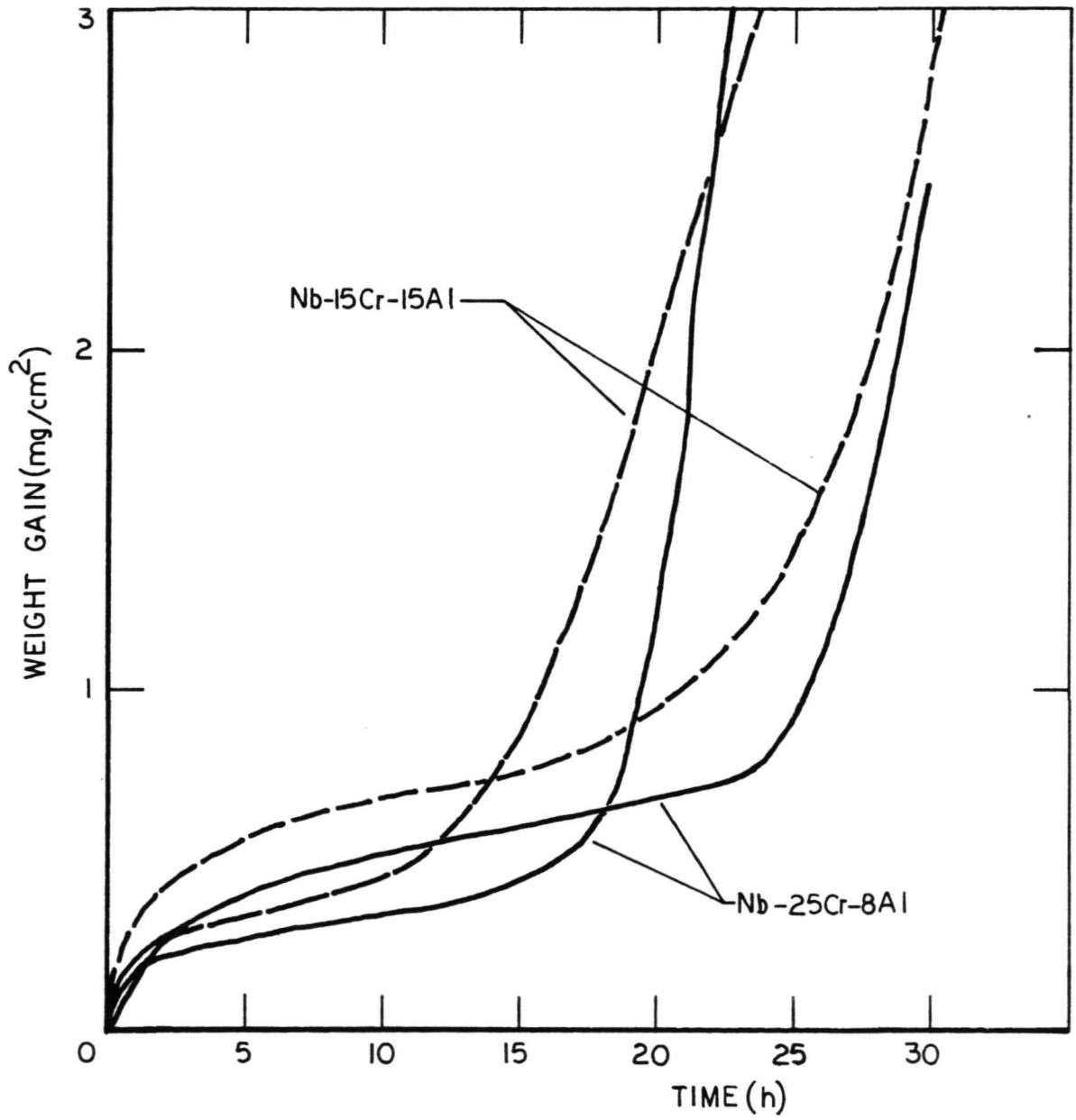
FIGURE 11. ISOTHERMAL OXIDATION KINETICS OF Nb-Cr-Al ALLOYS
AT 922K (1200°F) IN 1.33 x 10^4 N/m^2 (100 torr) AIR

TABLE 7. DETAILS OF Nb-Ti-Cr-Al ALLOY OXIDATION TESTS AT 922 K (1200°F) IN 1.33 x 10^4 N/m^2 (100 torr) AIR

Alloy	Specimen No.	Exposure Time s	Exposure Time h	Weight Gain (kg/m^2 x 10^2) Cahn	Weight Gain (kg/m^2 x 10^2) Check Weighing	Rate Index n*	Remarks
Nb-15Cr-15Al	16	1.44 x 10^4	4	--	-0.46	--	Balance failed
	17	1.15 x 10^5	32	3.67	3.66	2.7 (1-15 h)	
	32	1.8 x 10^5	50	10.43	10.65	~3 (1-8 h)	
Nb-25Cr-8Al	19	--	--	--	--	--	Coupon disintegrated
	20	2.16 x 10^4	6	2.98	2.11	--	
	29	8.64 x 10^4	24	3.75	--	{1.0 (0-1 h), 3.4 (1-9 h)	Coupon disintegrated on cooling
	31	1.08 x 10^5	30	2.47	0.38	{1.0 (0-2 h), 2.6 (2-18 h)	
Nb-42Ti-9Cr-6.5Al	48	4.21 x 10^5	117	0.29	0.37	1.3 (0-6 h)	
	49	2.45 x 10^5	68	0.31	0.18	{2.0 (0-6 h), > 2 (6-68 h)	
Nb-40Ti-9Cr-4Al	11	3.6 x 10^5	100	0.98	0.79	{2.0 (0-10 h), 2.9 (10-100 h)	
	10	2.48 x 10^5	69	0.66	0.63	2.1 (0-69 h)	
Nb-42Ti-4Cr-4Al	38	3.67 x 10^5	102	2.66	2.65	1.5 (0-44 h)	
	47	3.53 x 10^5	98	0.92	1.01	{3.5 (0-2 h), 2.0 (2-98 h)	
	41	9.0 x 10^4	25	0.59	0.59	1.5 (4-25 h)	1.01 x 10^5 N/m^2 (760 torr)
	43	1.78 x 10^5	49.5	0.54	0.61	--	Cyclic, 1.01 x 10^5 N/m^2 (760 torr)

* From w^n = kt where w = weight gain, t = time, and n, k are constants.
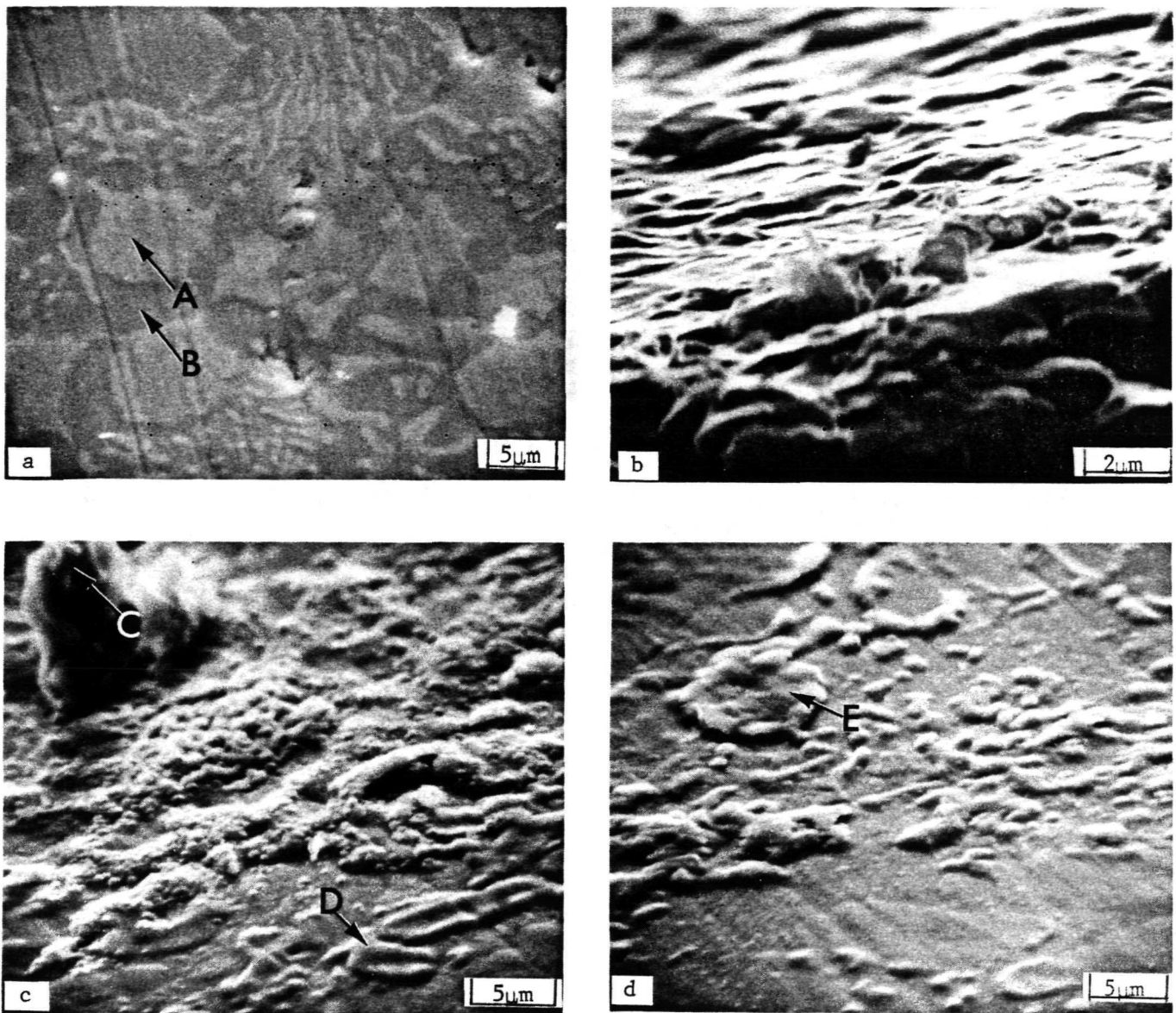
FIGURE 12. SCALES FORMED ON Nb-25Cr-8Al AFTER OXIDATION AT
922K (1200°F) FOR 1.07 x 10⁵ s (29.7 h) IN 1.33 x
10⁴ N/m² (100 torr) AIR

(a) Oxidized surface, with alloy phases visible through scale,
0.401 rad. tilt. Phase A: Nb:Cr:Al = 100:19:13; Phase B:
Nb:Cr:Al = 100:77:20.

(b) Oblique view of surface oxide, showing platelets and
mounds, 1.361 rad. tilt.

(c) Further view of platelets (C: Nb:Cr:Al = 100:63:23) and
mounds (D: Nb:Cr:Al = 100:22:17), 1.012 rad. tilt.

(d) Mounds of oxide which appear to be associated with dark (B)
phase. Mound E gave an analysis of Nb:Cr:Al = 100:19:19,
1.012 rad. tilt.

It therefore appears possible to form protective replacement scales on these alloys, but at the chromium and aluminum levels required the alloys are unsuitably brittle. Recently computed phase diagrams for the Nb-Cr-Al system[14] indicated that alloys which are single phase at 1273 K (1832°F) contain too little chromium (< 3.7) or aluminum (< 2.9) to form replacement scales, and at 922 K (1200 F) the single phase field will probably shift to lower chromium and aluminum levels. The maximum aluminum content of single-phase (β) Nb-Ti-Al alloys at 922 K is reportedly 4.8 weight percent[15], while β-alloys based on Ti-Nb-Cr-Al[16,17] (no compositions given), and on Ti-5.5Cr-3Al[18] possess good ductility, and have good oxidation resistance at 922 K from the formation of essentially TiO + TiO_2 scales.

The oxidation kinetics of the three β-type Nb-Ti-Cr-Al alloys investigated are shown in Figure 13 and Table 7. These alloys oxidized more slowly than pure titanium or Ti-6-2-4-2 at 922 K (1200°F) in 1.33×10^4 N/m² (100 torr) air and, as expected, the rates decreased with increasing aluminum content. The parabolic rate constants listed for these alloys in Table 4 refer only to the initial stages of oxidation, and do not indicate the long-term oxidation behavior. These alloys all formed thin, apparently adherent scales (Figure 14), which were colored either gold or purple, and which gave X-ray diffraction patterns attributable mainly to TiO_2. The surface topography of the scale formed on the Nb-40Ti-9Cr-4Al alloy, shown in Figure 14a, in fact appeared wrinkled and cracked, but it is probable that the wrinkling occurred on cooling, since the attack beneath these wrinkles (Figure 14b) is no more severe than elsewhere.

The scale formed on the most ductile of these β-type alloys, Nb-42Ti-4Cr-4Al, resisted spallation in a cyclic oxidation test, and the oxidation rate of this alloy was not greatly affected by increasing the air pressure from 1.33×10^4 N/m² (100 torr) to 1.01×10^5 N/m² (760 torr).

In summary, alloys based on Nb-Cr-Al can be used to form protective scales of alumina, but alloy compositions with this capability are very brittle in bulk form. The more ductile, β-type Nb-Ti-Cr-Al-base alloys form modified TiO_2 instead of alumina scales and can offer equivalent oxidation resistance to Ti_3Al as measured by weight-gain kinetics, but have superior ductility in bulk form to the titanium aluminides.

B. Hot-Salt Stress-Corrosion Evaluation

(i) Uncoated Ti-6Al-2Sn-4Zr-2Mo and Ti-5Al-6In-1.5Mo-0.5V Alloys. Tests to determine base-line hot-salt stress-corrosion data for these two alloys were carried out by exposing salted and unsalted specimens to a creep test at various stress levels for 3.6×10^5 s (100 h) at 755 K (900°F). A sodium chloride coating weight of 3×10^{-3} kg/m² was used throughout, and was applied by spraying a 0.7N solution of the salt onto the test sections of the coupons preheated to about 393 K (248°F). The specimen size of 0.102 m (4 inches) length by 0.025 m (1 inch) wide (shoulders), with a 0.006 m
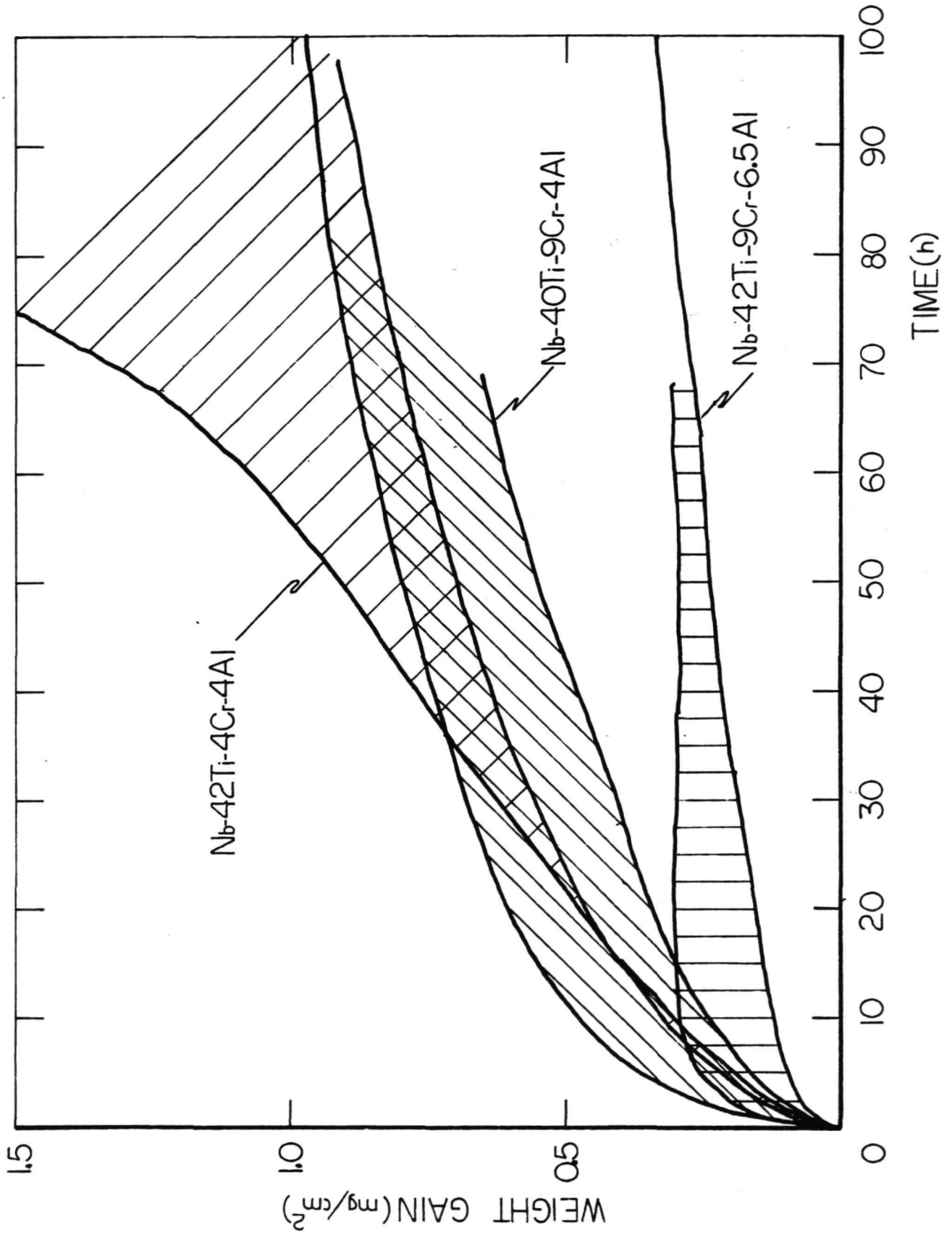
FIGURE 13. OXIDATION KINETICS OF Nb-Ti-Cr-Al ALLOYS AT 922 K (1200°F) IN 1.33 x 10^4 N/m^2 (100 TORR) AIR
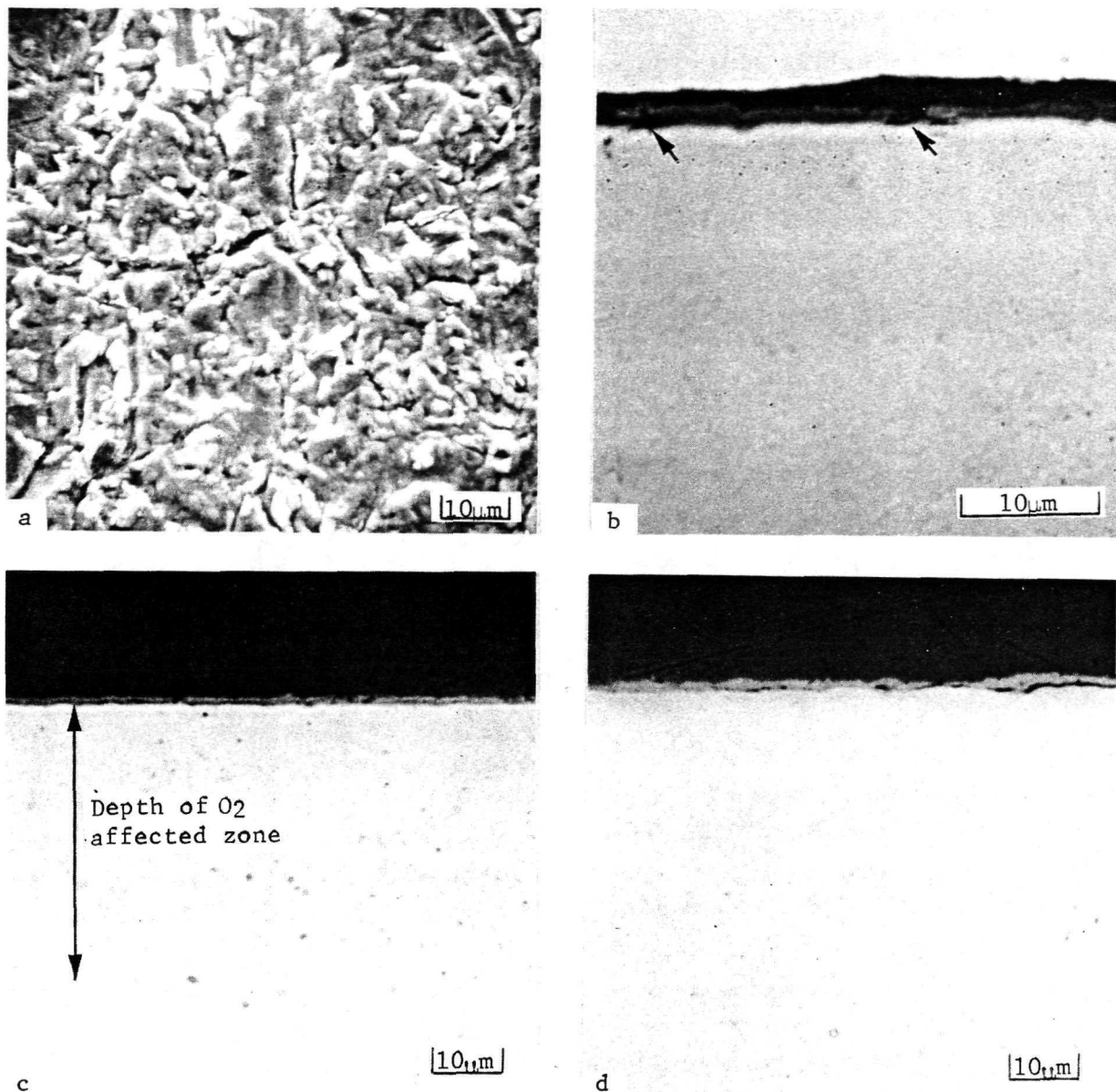
FIGURE 14. OXIDE SCALES FORMED ON Ti-Nb-Cr-Al ALLOYS OXIDIZED
AT 922 K (1200°F) IN 1.33 x 10^4 N/m^2 (100 torr) AIR

(a) Topography of scale formed on Nb-40Ti-9Cr-4Al Alloy after 2.48 x 10^5 s
(69 h) at 922 K (1200°F) in 1.33 x 10^4 N/m^2 (100 torr) air. Back
scattered electron image at 0.506 rad. tilt (No. 10).

(b) Cross section of scale shown in (a). The arrows indicate wrinkles in the
scale which are similar to those shown in (a). The O_2 affected zone in
this alloy extends beyond the depth of alloy matrix shown.

(c) Cross section of scale formed on Nb-42Ti-9Cr-6.5Al after 4.21 x 10^5 s
(117 h) at 922 K (1200°F) in 1.33 x 10^4 N/m^2 (100 torr) air.

(d) Cross section of scale formed on Nb-42Ti-4Cr-4Al after 3.53 x 10^5 s
(98 h) at 922 K (1200°F) in 1.33 x 10^4 N/m^2 (100 torr) air. The O_2-
affected zone in this alloy extends beyond the depth of alloy matrix
shown.

(0.25 inch) by 0.025 m (1 inch) reduced section was used in all cases where the test material was available in sheet form. The embrittling effect of the heat treatment and the salt coating were assessed by post-test room temperature tensile tests, the results of which are given in Tables 8 and 9.

The data for the unsalted Ti-6-2-4-2 specimens, which were gathered to determine the tensile stress level required to produce 0.2 percent plastic strain, suggest that this alloy is somewhat less creep-resistant than reported in the literature, which indicated that a stress of about 380 MN/m^2 (55 ksi) would have been required to produce 0.2 percent plastic strain under the test conditions. The hot-salt test data for the Ti-6-2-4-2 alloy confirmed earlier data[2], and suggest that the base sheet alloy has no real corrosion threshold stress in this test. These results represent a confusing material behavior. Salted specimens exposed at low stress levels, 0, 69, and 103 MN/m^2 (0, 10, and 15 ksi) showed surface pitting after the creep exposure and exhibited an embrittled condition in the post-creep room-temperature tensile test (less than 50 percent of the unexposed ductility). No hot-salt cracks were observed on the fracture surfaces of these specimens. A specimen exposed in creep at 138 MN/m^2 (20 ksi) showed surface pitting but was found to be ductile in post-creep tensile testing (specimen No. 8). A specimen exposed at a stress of 207 MN/m^2 (30 ksi) showed severe surface pitting and was brittle in the post-creep tension test. Failure occurred at a typical "hot-salt" crack which intruded about 0.0007 m from one edge.

The hot-salt stress-corrosion threshold stress for the uncoated Ti-5-6-1.5-0.5 alloy in this test appears to lie between 138 and 172 MN/m^2 (20-25 ksi). This alloy therefore appears more resistant to this test than Ti-6-2-4-2 sheet, although less creep resistant at 755 K (900°F).

(ii) Ti-6Al-2Sn-4Zr-2Mo Sheet with TRW Coatings. In an earlier program[2], performed by TRW, Inc., several promising coating compositions intended to provide environmental protection to 922 K (1200°F) were applied to Ti-6-2-4-2 sheet. Of these, coating Number 2: Si (slurry), Number 3: Cr (slurry) over Al-Mg (pack) and Number 5: Al-Mg (pack) were available for testing. These coatings appeared to be quite uniform in thickness, dense, and adherent to the alloy surface. However, the as-received coatings contained a few cracks which penetrated to the substrate. After testing (hot salt plus room temperature tensile) these were more numerous, some appeared to have propagated into the substrate, and others to have served as sites for corrosive attack.

The hot-salt stress-corrosion test results in Table 10 for the coated alloy in fact suggest that the susceptibility to attack is increased. Detailed examination of the coatings suggested reasons for this behavior. Figure 15a shows a cross section of the shoulder of a silicon slurry-coated coupon after room temperature tensile testing only. Cracks in the coating run almost normal to the coating thickness through the outer part of the coating, shown in Figure 16a to be possibly TiSi (44 Si, 47 Ti), and then on entering the inner part of the coating (possibly Ti_5Si_3, 23 Si, 66 Ti) turn to follow the coating/substrate interface. This coating then is apparently quite brittle, so that the protection provided by its barrier layer action was probably negated by cracking under load.

TABLE 8. LONGITUDINAL CREEP AND TENSILE PROPERTIES OF UNCOATED Ti-6Al-2Sn-4Zr-2Mo ALLOY

Specimen Number	Condition	Creep Exposure Data 755K (900°F)					Room Temperature Tensile Test Data					
		Time sec	Time hrs	Stress MN/m²	Stress ksi	Plastic Strain, %	UTS MN/m²	UTS ksi	YS MN/m²	YS ksi	El, %	RA, %
A	As received	No exposure					79	142	862	125	15	29
B	As received	No exposure					79	142	862	125	14	26
1	As received	3.6x10⁵	100	276	40	0.344	1076	156	938	136	14	27
2	As received	3.6x10⁵	100	241	35	0.256	1076	156	958	139	15	26
3	As received	3.6x10⁵	100	207	30	0.208	1089	158	972*	141	15	24
4	Salted	3.6x10⁵	100	207	30	0.228	910	132	Br.	--	2	13
12	Salted	3.6x10⁵	100	172	25	0.157	593	86	--	--	0	0
8	Salted	3.6x10⁵	100	138	20	0.120	1089	158	986	143	11	16
9	Salted	3.6x10⁵	100	117	17	0.130	1089	158	1000	145	13	24
5	Salted	3.6x10⁵	100	103	15	0.096	1069	155	993	144	6	15
11	Salted	3.6x10⁵	100	103	15	0.065	1048	152	979	142	5	11
7	Salted	3.6x10⁵	100	69	10	0.040	1082	157	1007	146	7	14
6	Salted	3.6x10⁵	100	0	0	--	1069	155	1007	146	7	16
		922K (1200°F)										
13	As received	3.6x10⁵	100	7	1	0.265	951	138	924	134	6	--
14	As received	3.6x10⁵	100	7	1	0.309	979	142	917	133	10	--
10	As received	3.6x10⁵	100	17	2.5	0.988	979	142	903	131	12	16

* Broke before reaching 0.2%YS.

TABLE 9. LONGITUDINAL CREEP AND TENSILE PROPERTIES OF UNCOATED
Ti-5Al-6In-1.5Mo-0.5V ALLOY

Specimen Number	Condition	755K (900°F) Creep Exposure Data					Room Temperature Tensile Test Data					
		Time		Stress		Plastic Strain, %	UTS		YS		Fl, %	RA, %
		sec	hrs	MN/m²	ksi		MN/m²	ksi	MN/m²	ksi		
V4623-0	As received	No exposure		No exposure			1020	148	938	136	18	34
-1	As received	No exposure		No exposure			979	142	876	127	15	34
-2	As received	3.6x10⁵	100	207	30	0.356	972	141	896	130	16	37
-3	As received	3.6x10⁵	100	172	25	0.304	958	139	876	127	18	31
-5	As received	3.6x10⁵	100	138	20	0.196	986	143	903	131	15	31
-6	Salted	3.6x10⁵	100	172	25	0.27	524	76	--	--	~1	~2
-4	Salted	3.6x10⁵	100	138	20	0.187	1076	156	903	131	14	27

TABLE 10. LONGITUDINAL CREEP AND TENSILE PROPERTIES OF Ti-6Al-2Sn-4Zr-2Mo SHEET WITH TRW COATINGS

Specimen Number	Coating Type	Condition	755K (900°F) Creep Exposure Data					Room Temperature Tensile Test Data					
			Time		Stress		Strain, %	UTS		YS		El, %	RA, %
			sec	hrs	MN/m²	ksi		MN/m²	ksi	MN/m²	ksi	%	%
							S1 Slurry Coating (TRW No. 2)					
2-1	Si	No salt	No exposure					834	121	745	108	12	20
2-2	Si	No salt	3.6x10⁵	100	172	25	0.074	855	124	807	117	6	14
2-5	Si	Salted	3.6x10⁵	100	172	25	0.100	593	86	586	85	2	8
2-7	Si	Salted	3.6x10⁵	100	138	20	0.065	545	79	--	--	<1	~2
			Cr Slurry + Al-Mg Pack Coating (TRW No. 3)										
3-1	Cr+Al/Mg	No salt	No exposure					938	136	931	135	2	10
			Al-Mg Pack Coating (TRW No. 5)										
5-1	Al/Mg	No salt	No exposure					889	129	807	117	13	22
5-2	Al/Mg	No salt	3.6x10⁵	100	172	25	0.048	917	133	834	121	12	16
5-3	Al/Mg	Salted	2.2x10³	0.6	172	25	0.36*	Failed in creep test					
5-4	Al/Mg	Salted	5.0x10³	1.4	138	20	2.6*	Failed in creep test					
5-5	Al/Mg	Salted	8.6x10³	2.4	69	10	0.4*	Failed in creep test					

* Total Strain.
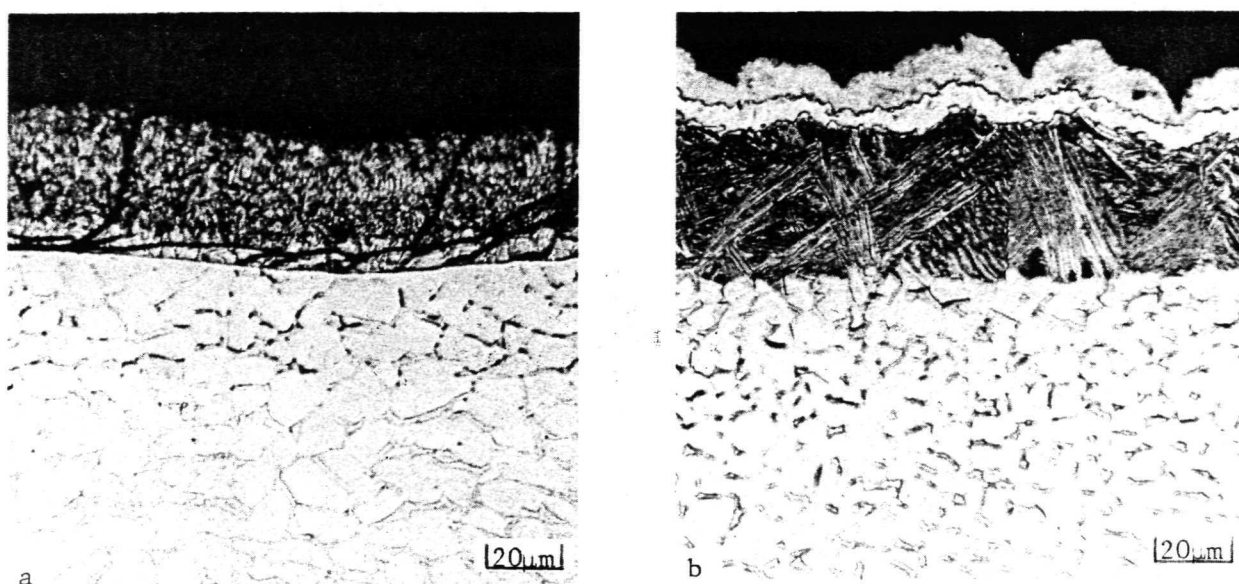
FIGURE 15. CROSS SECTIONS OF COATINGS ON Ti-6Al-2Sn-4Zr-2Mo ALLOY

(a) Si slurry coating (TRW No. 2), as received,
     tensile tested (Specimen No. 2-1)

(b) Cr slurry + Al-Mg pack coating (TRW No. 3),
     as received, tensile tested (Specimen No. 3-1)
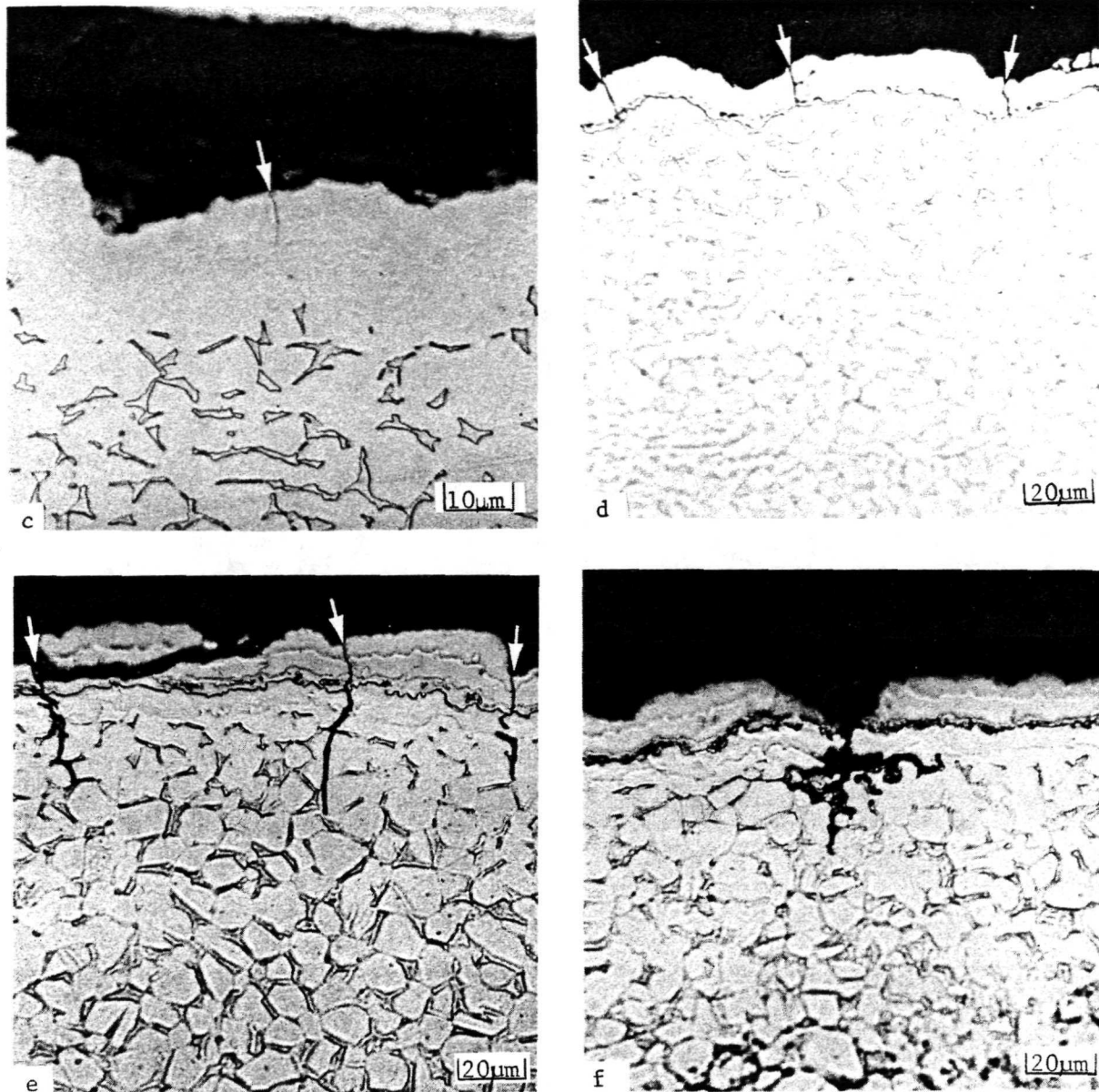
FIGURE 15. (Continued)

(c) As received, Al-Mg pack coating, etched, showing typical crack in coating (TRW No. 5-6)

(d) As received, Al-Mg pack coating, showing typical crack distribution in coating, after tensile testing at room temperature (TRW No. 5-1)

(e) After hot-salt stress-corrosion test, area near point of failure in post-test tensile test (TRW No. 5-4)

(f) After hot-salt stress-corrosion test, area remote from post-test failure site (TRW No. 5-6)
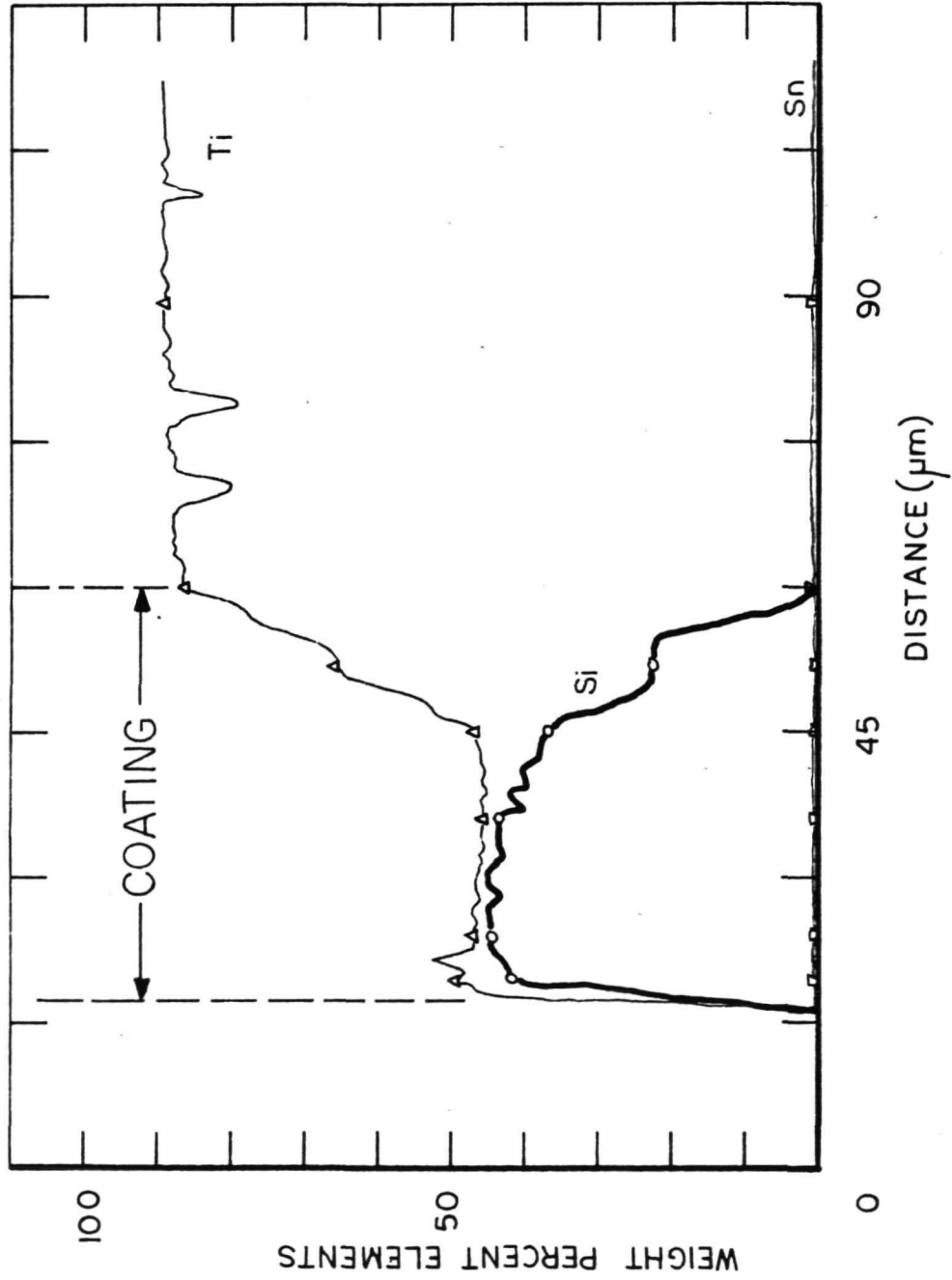
FIGURE 16a. CONCENTRATION PROFILES THROUGH Si SLURRY COATING
(TRW NO. 2) ON Ti-6-2-4-2. (Specimen 2-1)
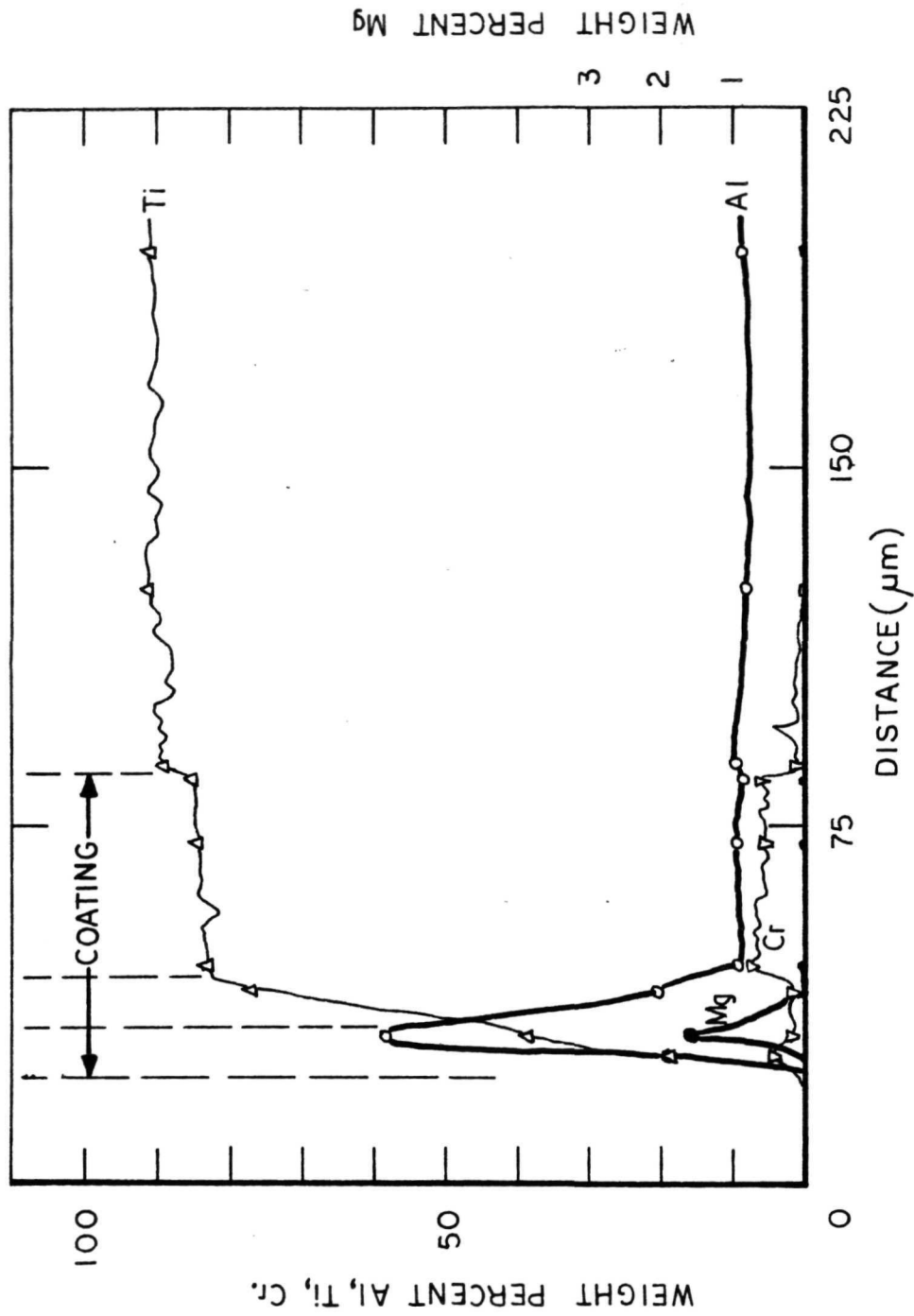
FIGURE 16b.   CONCENTRATION PROFILES THROUGH Cr SLURRY + Al/Mg PACK COATING
(TRW NO. 3) ON Ti-6-2-4-2 (Specimen No. 3-1)
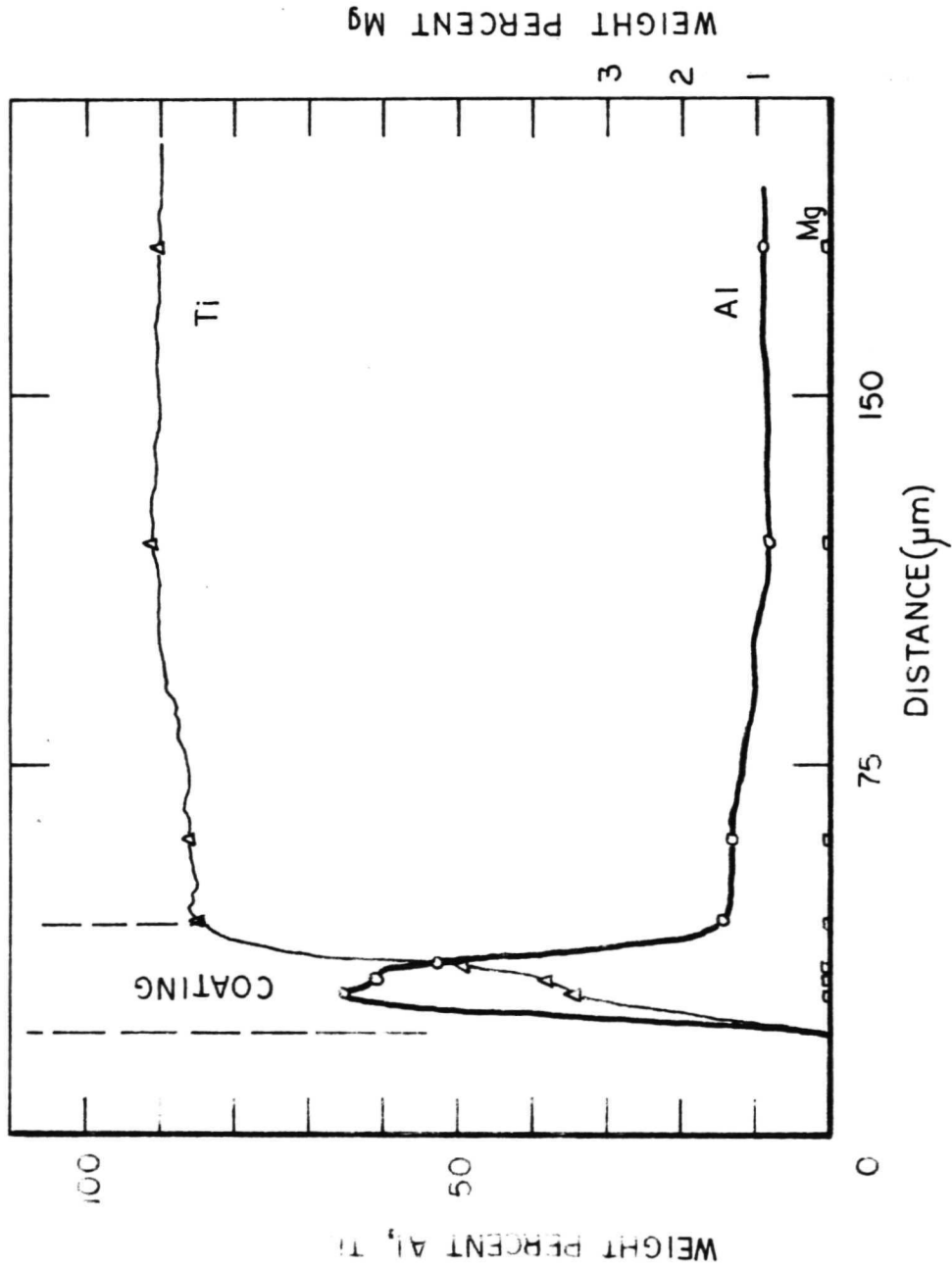
FIGURE 16c. CONCENTRATION PROFILES THROUGH Al-Mg PACK COATING
(TRW NO. 5) ON Ti-6-2-4-2 (Specimen NO. 5-1)

The Cr slurry + Al/Mg pack coating, shown in Figure 15b, exhibited relatively few cracks, although the depth of the chromium-stabilized beta zone, shown as the dark-etching layer with acicular structure, was considerable. The approximate locations of the three layers of this coating are indicated in the concentration profile in Figure 16b, which also shows the maximum magnesium content found (around 1.7 weight percent). It must be emphasized that magnesium was present in the coating in small, localized spots, and that the area shown in Figure 16b was located by careful searching.

The Al-Mg pack coating is shown in Figures 15c to 15f. Figure 15c shows a typical crack occurring in the as-received coating (arrows), and Figure 15d shows the frequency of cracking after tensile testing, and the penetration of some cracks toward the substrate. Figure 15e shows the further penetration of such cracks into the substrate after exposure to the hot-salt stress-corrosion test (and subsequent room temperature tensile testing), and Figure 15f shows corrosion attack of the substrate beneath what had apparently been a crack in the coating, at a site remote from the point of failure in the tensile test. It had been hoped that such attack would have been minimized by the presence of the electrochemically-active magnesium in the coating but, as is shown in Figure 16c, virtually no magnesium (0.2 weight percent) was detected.

In view of these unsatisfactory physical and chemical features of these coatings, evaluation of them was terminated.

(iii) <u>Separate Phase Alloys for Consideration as Coatings</u>. The titanium literature contains many examples of the use of apparently simple coating systems, such as aluminum[3, 19-23], or nickel[19-21, 23-26] for protection against hot-salt stress-corrosion, but often the results of exposure tests are contradictory. Although the effects of variables such as method of application of a coating or differences in alloy substrate on the effectiveness of even simple coatings have not been well characterized, there is some evidence that the more ductile intermetallic compounds formed between the simpler coatings and the substrate are to be preferred.

In this approach, the hot-salt stress-corrosion behavior of several such alloys was investigated:

(a) Ti-55Ni   barrier layer of good ductility,
     Nb-42Ti-4Cr-4Al   protected by modified TiO_2 scales.

(b) Ti-16Al   barrier layer of limited ductility,
     Ti-35Al   protected by modified TiO_2 scales.

(c) Ti-63Al   barrier layer of limited ductility,
                                     protected by alumina scales.

(a) <u>Ductile Barrier Layer Alloys</u>. The two alloys considered in this category are available in sheet form, so that tests were performed on standard tensile test pieces cut from sheet. The results for the Ti-55Ni alloy in Table 11 indicate that it is little affected by the salt, even though the oxygen-contamination zone is brittle and cracks under load, as shown in Figure 17a.

The Nb-40Ti-4Cr-4Al alloy did suffer embrittlement in this test (Table 12) although no hot-salt cracks were observed in the failed areas. However, in places the oxygen-contaminated subscale was found to be cracked (Figure 17b) with some cracks penetrating the alloy substrate.

(b) <u>Barrier Layer Alloys With Limited Ductility</u>. Tensile test bars were prepared from the Ti-16Al and Ti-35Al alloys by machining from cast finger ingots. These specimens had test sections 6.35×10^{-3} m (0.25 inch) in diameter by 3.81×10^{-2} m (1.5 inch) long, with an overall length of 9.53×10^{-2} m (3.75 inch). The results of hot-salt stress-corrosion exposures on these alloys, listed in Table 13, suggest that both are subject to hot-salt cracking. The threshold stress for Ti-16Al lies between 83 and 52 MN/m^2 (12 and 7.5 ksi), while that for the Ti-35Al alloy probably lies around 207 MN/m^2 (30 ksi).

Hot-salt cracks were observed in the Ti-16Al specimens which failed in the test (Figure 18d), and in the Ti-35Al specimen exposed initially at 207 MN/m^2 (30 ksi) and then at 310 MN/m^2 (45 ksi) until it broke. However, despite careful machining, these specimens were not free of notches resulting from casting defects, and the influence of these on the hot-salt stress-corrosion behavior is unknown.

Exposure of small, flat unstressed specimens of Ti-16Al to the conditions of this test indicated that degree of surface finish had a large effect on the extent of hot-salt corrosion. The cross sections in Figure 18 show that preferential attack of an aligned phase (possibly ϵ) in the transformed β phase occurs, possibly through electrochemical contrast. The depth of attack reached approximately 15 μm in a specimen roughly polished (80 grit) before exposure, but only approximately half this depth in a specimen polished through 600 grit. Post-test examination of Ti-16Al specimen number 20 which broke in the hot salt test (Table 13), indicated the presence of salt crystals on the failed surface, which showed signs of corrosive attack (Figure 18). In cross section this attack was seen to have the same form of preferential corrosion as that observed on the unstressed coupons.

The Ti-35Al composition used is not single phase, and preferential corrosion of one phase was observed in this alloy, Figure 19, the depth of penetration of this attack depending on the alignment of the microstructure. Coatings of this general composition might be rendered more resistant to hot-salt by using the single-phase alloy, Ti-40Al.

TABLE 11. LONGITUDINAL CREEP AND TENSILE PROPERTIES OF Ti-55Ni ALLOY

Specimen Number	Condition	755K (900°F) Creep Exposure Data					Room Temperature Tensile Test Data					
		Time		Stress		Plastic Strain,%	UTS		YS		El, %	RA, %
		sec	hrs	MN/m^2	ksi		MN/m^2	ksi	MN/m^2	ksi		
1	As received	3.6x10^5	100	34	5	0.868	1055	153	145	21	6	17
2	As received	3.6x10^5	100	14	2	0.309	1145	166	138	20	11	19
3	Salted	3.6x10^5	100	14	2	0.248	1000	145	145	21	6	17
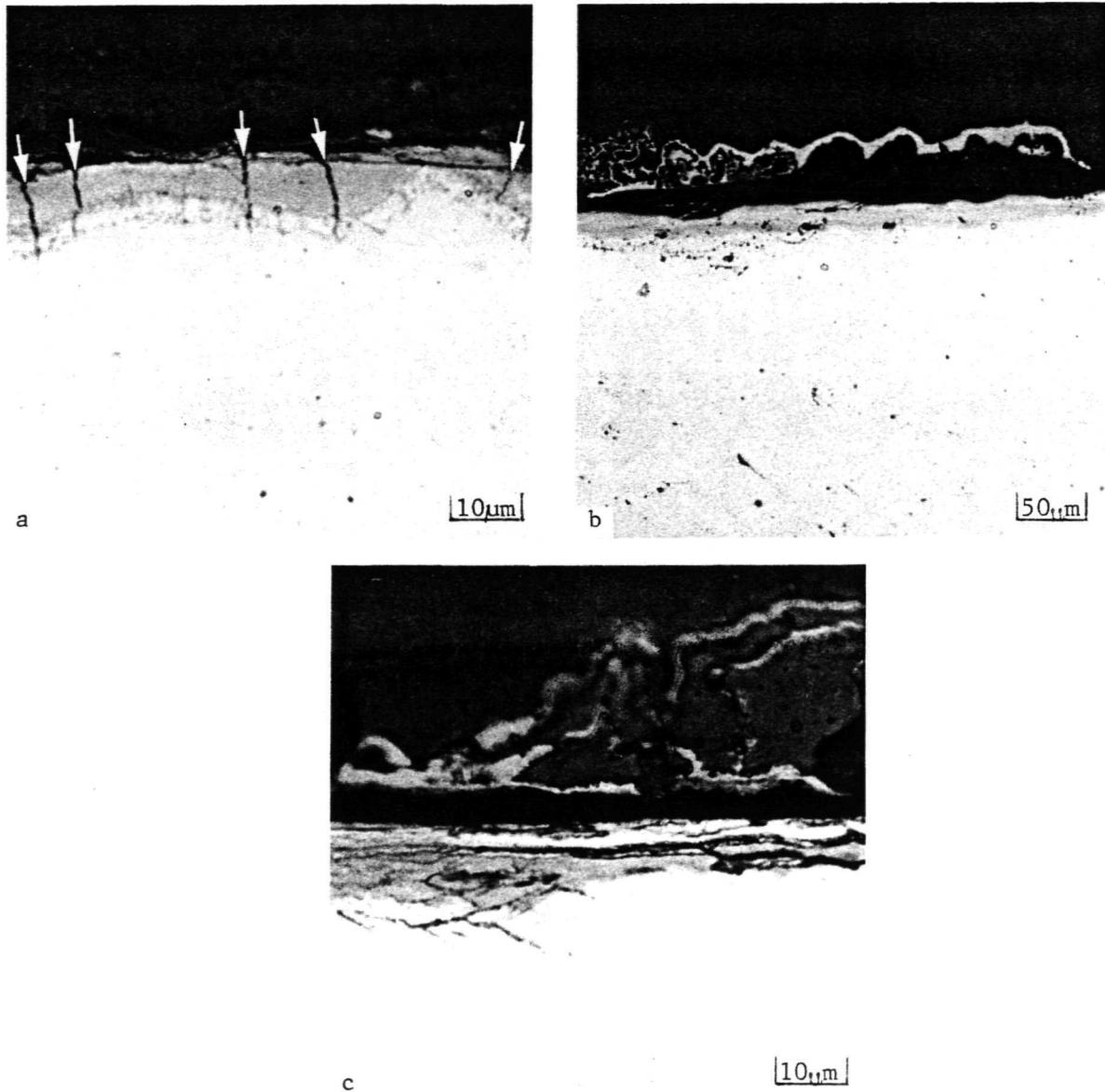
FIGURE 17. SCALE MORPHOLOGIES ON DUCTILE BARRIER LAYER ALLOYS
AFTER EXPOSURE IN HSSC TEST

(a) Ni-55Ti alloy after exposure at 14 MN/m^2 (2 ksi) and subsequent room temperature tensile testing, showing cracks in subscale

(b) Nb-42Ti-4Cr-4Al after exposure unstressed, showing external scale and extensive subscale

(c) Nb-42Ti-4Cr-4Al after exposure at 69 MN/m^2 (10 ksi) and subsequent room temperature tensile testing, showing cracked subscale

TABLE 12. LONGITUDINAL CREEP AND TENSILE PROPERTIES OF
Nb-42Ti-4Cr-4Al ALLOY

Specimen Number	Condition	Creep Exposure Data 755 K (900°F)					Room Temperature Tensile Test Data					
		Time		Stress		Strain, %	UTS		YS		Elong., %	R.A., %
		sec	hrs	MN/m²	ksi		MN/m²	ksi	MN/m²	ksi		
1	As rolled sheet	No exposure				--	1151	167	1089	158	5	16
2	As rolled sheet	3.6 x 10⁵	100	69	10	0.148	1496	217	1482	215	1	7
3	Salt	3.6 x 10⁵	100	69	10	0.157	607	88	--	--	1	4
4	Salt	3.6 x 10⁵	100	52	7.5	0.125	979	142	--	--	<1	3
5	Salt	3.6 x 10⁵	100	34	5	0.093	869	126	--	--	<1	4

TABLE 13. LONGITUDINAL CREEP AND TENSILE PROPERTIES OF
Ti-16Al AND Ti-35Al ALLOYS

| Alloy | Specimen Number | Condition | 755 K (900°F) Creep Exposure Data | | | | | Room Temperature Tensile Test Data | | | | | |
| | | | Time | | Stress | | Strain, | UTS | | YS | | El, | RA, |
			sec	hrs	MN/m²	ksi	%	MN/m²	ksi	MN/m²	ksi	%	%
Ti-16Al	18	As-cast and machined	3.6×10^5	100	103	15	0	145	21	--	--	1	2
	20	Salt	--	--	103	15	(Broke after 1.51×10^4 s (4.2 h))						
	19	Salt	3.6×10^5	100	52	7.5	0	131	19	--	--	~1	1
	22	Salt	--	--	83	12	(Broke in 9×10^3 s (2.5 h))						
Ti-35Al	23	As-cast and machined	3.6×10^5	100	172	25	0	393	57	--	--	2	3
	26	Salt	3.6×10^5	100	248	36	0.022	379	55	--	--	<1	<1
	25	Salt *	$\begin{cases}3.6 \times 10^5 \\ 3.51 \times 10^5\end{cases}$	$\begin{cases}100 \\ 97.4\end{cases}$	$\begin{cases}207 \\ 310\end{cases}$	$\begin{cases}30 \\ 45\end{cases}$	$\begin{cases}0.019 \\ \text{--}\end{cases}$	--	--	--	--	--	--
	24	Salt	3.6×10^5	100	172	25	0	379	55	--	--	<1	<1

* First exposure for 3.6×10^5 s at 207 MN/m² was followed by uninterrupted
exposure at 310 MN/m² until specimen failed in creep after 3.51×10^5 s.
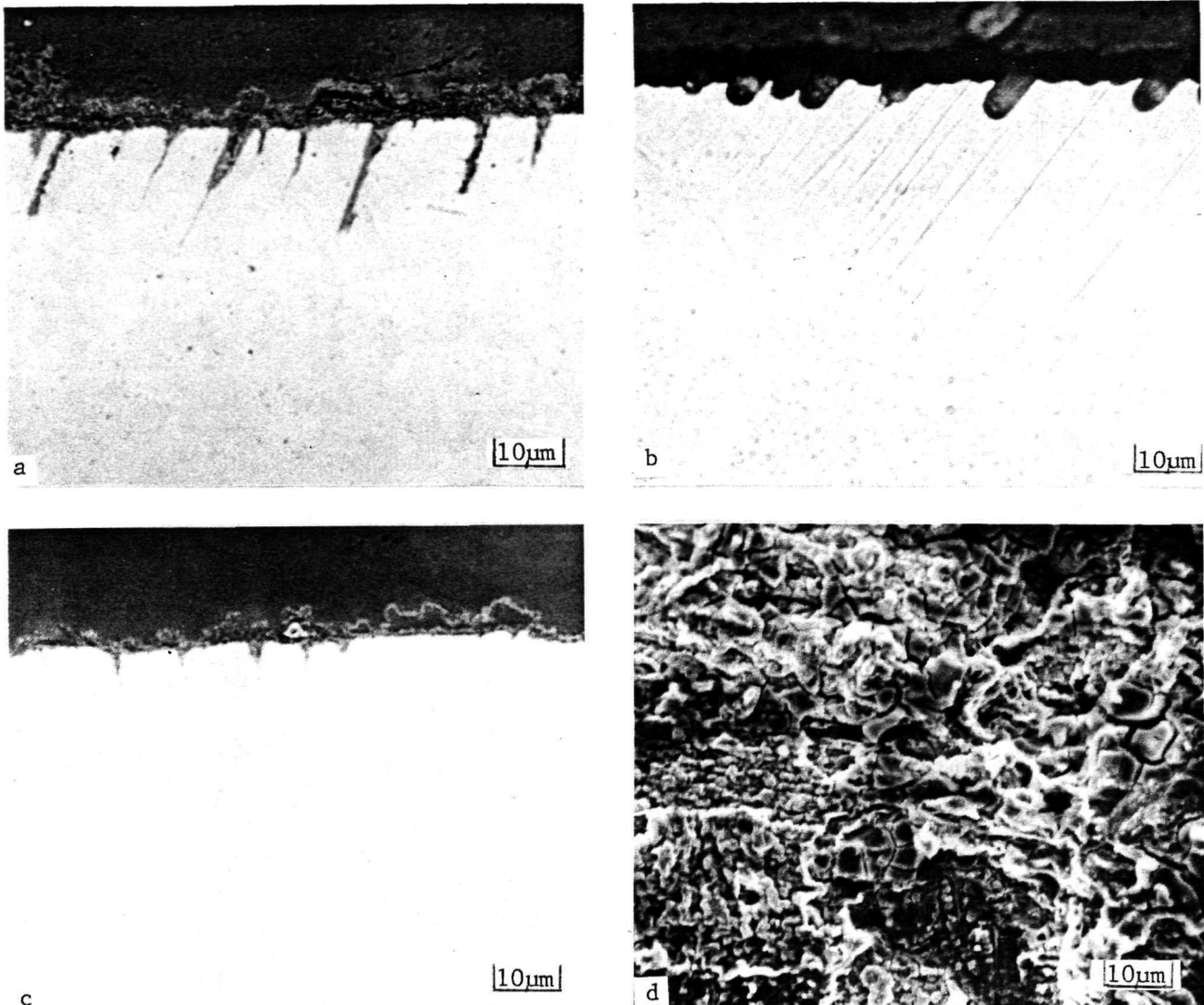
FIGURE 18.   SCALE MORPHOLOGIES ON Ti-16Al AFTER EXPOSURE IN HSSC TEST

(a)   Exposed unstressed, with surface polished through 80
grit showing oxide penetration to about 15 μm

(b)   Same as (a), etched to show preferential corrosion
of aligned phase (possibly ϵ) in the transformed β phase

(c)   Exposed unstressed, with surface polished through 600
grit, showing reduced oxide penetration

(d)   Scanning electron micrograph of fracture surface of
specimen No. 20 after failure during exposure at
103 MN/m^2 (15 ksi) creep stress, showing corrosion
attack
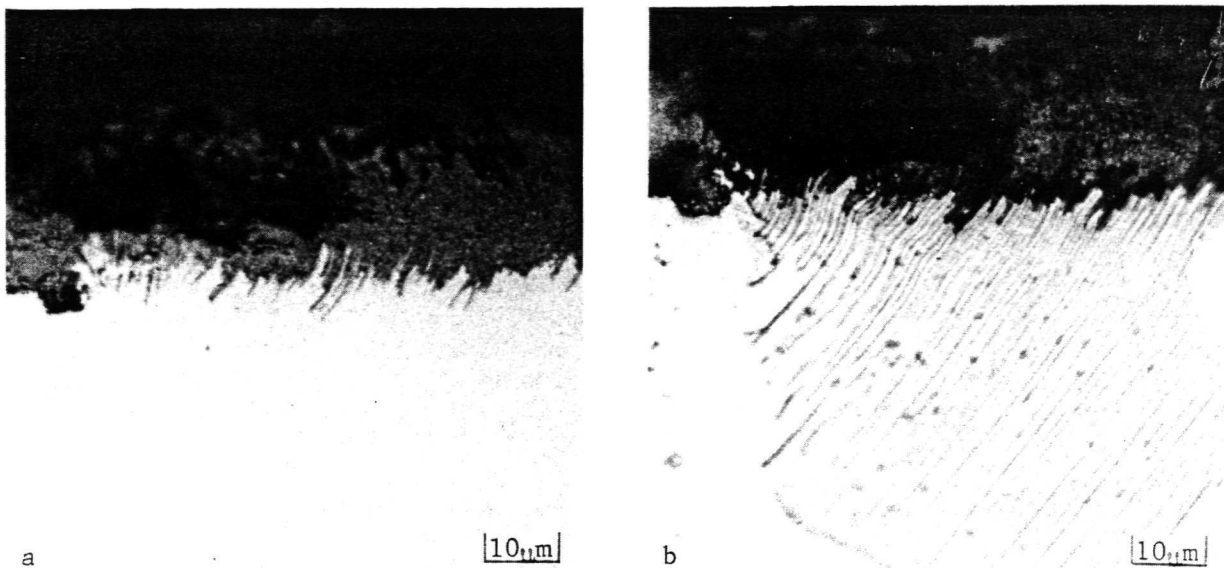
FIGURE 19. HOT-SALT ATTACK OF Ti-35Al

(a) Preferential attack of specimen No. 25, exposed 3.6×10^5 s
     at 207 MN/m^2 then 3.51×10^5 s at 310 MN/m^2 in HSSC test
     at 755 K (900°F)

(b) Same area as (a), etched to show relation of attack to
     microstructure

(iv) Coating Attempts

(a) Electrochemically-Active Coatings. The apparent effectiveness
of coatings of elements electrochemically much less noble than titanium in
combating hot-salt stress-corrosion, such as Mg[3], Zn[21,22], and Al, is the
basis of this approach. Because of the very low magnesium content of the TRW
coatings, an attempt was made to pack diffuse magnesium into the surface
regions of Ti-6-2-4-2 coupons as an alternative means of examining the effect
of electrochemical suppression of the titanium-salt corrosion reaction. The
pack comprised 0.35 kg MgO, 0.0125 kg Mg powder, 0.0025 kg NaCl, and 0.0025 kg
urea, and the diffusion treatment lasted 8.64×10^4 s (24 h) at 1227 K (1750°F).
Electronprobe microanalysis of the resulting surface structure, shown in
Figure 20a, failed to detect any magnesium. A layer some 100 μm thick at the
surface of the specimens contained appreciable porosity, and was enriched in tin
and depleted in titanium. No attempt was made to check the aluminum, zirconium,
or molybdenum levels of this layer.

Considerable effort was expended in an attempt to melt and cast
titanium alloys containing magnesium or zinc. Direct arc-melting of a
Ti-4Zn composition was unsuccessful. A Ti-80Zn master alloy was suc-
cessfully melted and cast, but in subsequent arc-melting to form a Ti-10Zn
alloy, the zinc was volatilized. In the course of this work, some wetting
of a Ti-35Al alloy by molten magnesium was observed, but this proved to be
irregular and often associated with oxide dross fragments from the bath.

(b) Intermetallic Diffusion Coatings. Attempts were made to pack
aluminize coupons of Ti-6-2-4-2 to form the intermetallics TiAl and Ti$_3$Al in
the surface regions. Interdiffusion between aluminum and titanium alloys
produces only the TiAl$_3$ intermetallic[27], so that in this case the pack used
in an attempt to form a TiAl coating comprised alumina, urea, sodium chloride,
and Ti-63Al powders, in the weight proporations of 92.2:1:1:5.7, and in that
used in an attempt to form a Ti$_3$Al coating Ti-20Al powder was substituted
for Ti-63Al. Diffusion runs were made for 2.16×10 s (6 h) at 1227 K (1750°F),
the temperature being chosen to avoid α-β transformation in the alloy. Metal-
lographic and electron microprobe examination of the specimens before and after
the pack treatment, however, revealed that little diffusion of aluminum had
occurred.

An investigation of the factors involved led to the conclusion that
the temperature of the pack anneal was too low to effect significant aluminum
diffusion in the time allowed. Diffusion in this system is apparently very
temperature-dependent: an aluminized layer approximately 15 μm thick was
formed on a Ti-6Al-4V alloy after 2.16×10^4 s (6 h) at 1255 K (1800°F) in
the pack containing Ti-20Al[28]. This same aluminized alloy, however, also
contained a rim, some 100 μm thick, of stabilized α phase as a result of
oxygen and nitrogen uptake during the pack annealing treatment.
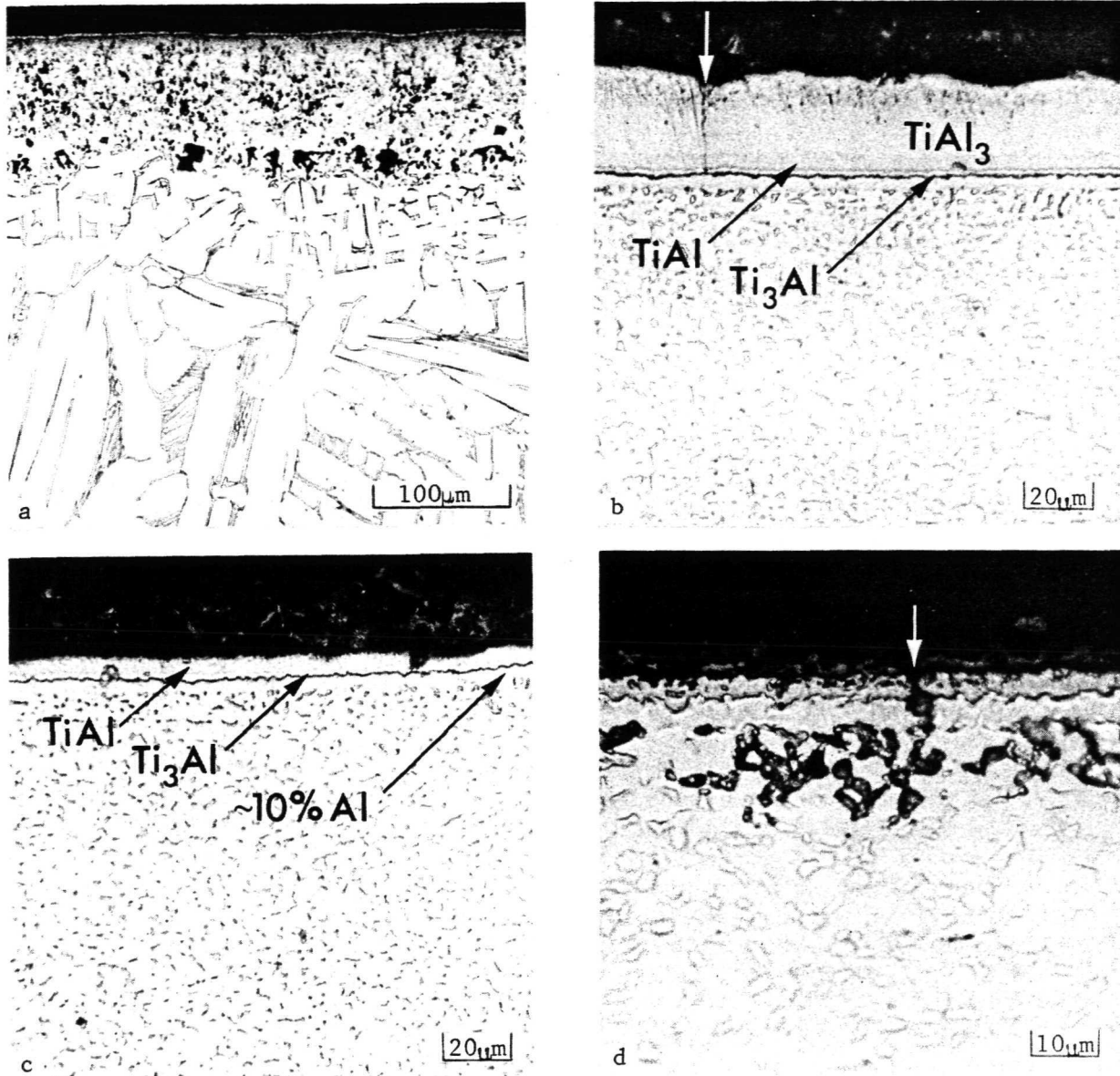
FIGURE 20. CROSS SECTIONS OF COATINGS ON Ti-6-2-4-2

(a) Surface of Ti-6-2-4-2 alloy after attempt to pack diffuse Mg

(b) Coating produced by annealing hot-dipped Al coating for 2.23×10^5 s (62 h) at 922 K (1200°F)

(c) Coating produced by annealing hot-dipped Al coating for 2.23×10^5 s (62 h) at 922 K (1200°F) followed by 8.64×10^4 s (24 h), at 1089 K (1500°F)

(d) Attack of Al/TiAl$_3$ coating which failed after 9.9×10^4 s (27.5 h) exposure in HSSC test (specimen No. 20)

(c) <u>Intermetallic Coatings by Hot Dipping and Diffusion</u>. Coatings of titanium-aluminum intermetallics were formed on tensile test specimens of the Ti-6-2-4-2 alloy by dipping in molten aluminum and annealing, using data from van Loo and Rieck[27]. By metallographic and electron microprobe examination of dipped and annealed specimens, it was determined that conditions required to convert the as-dipped coating to $TiAl_3$ (for coatings up to 30 μm thick) were a 10 s dip in molten aluminum at 1073 K (1472°F) followed by an anneal for 2.23×10^5 s (62 h) at 922 K (1200°F). TiAl coatings were produced from the $TiAl_3$ coatings by a further anneal at 1089 K (1500°F) for 8.64×10^4 s (24 h).

Some typical coatings are shown in Figure 20. Uniformity of the coatings was not well controlled over the specimen length, and in the thicker coatings some cracks were observed. During exposure to the hot-salt test some interdiffusion of the as-dipped coatings with the substrate occurred to form a layer of $TiAl_3$ at the alloy/coating interface, which may have contributed to embrittlement and cracking of the coating.

The results of exposing these specimens with as-dipped aluminum ($Al/TiAl_3$) coatings or with TiAl coatings to the hot-salt stress-corrosion test are shown in Table 14. The presence of an as-dipped or dipped and annealed coating had little or no effect on the room temperature tensile properties of the Ti-6-2-4-2 alloy, either before or after an <u>unsalted</u> creep exposure under the test conditions. In addition the annealing treatment did not affect the hot-salt performance of uncoated Ti-6-2-4-2. However the coated alloy was extremely sensitive to hot-salt stress-corrosion, specimens with the as-dipped aluminum coating did not survive the creep test even at a stress of 103 MN/m^2 (15 ksi), and the specimens with the TiAl coating failing at stresses as low as 69 MN/m^2 (10 ksi). Post-test examination of the coatings showed a mode of failure similar to that observed for the TRW Al-Mg pack coating (see Figure 15f), with preferential corrosive attack of the transformed β - phase of the Ti-6-2-4-2 alloy beneath apparent cracks in the coating (Figure 20d). Failures were often associated with areas of thin coatings (5-10 μm), the thicker areas of coatings showing little sign of attack. From these observations it was concluded coating imperfections and irregularities were the most likely cause of failure in the HSSC test, allowing localized access of salt to the substrate.

C. <u>Oxygen Contamination Evaluation</u>

The prime function of the oxygen contamination test was intended to be a test of the effectiveness of a coating while held in tension at 922 K (1200°F) for 3.6×10^5 s (100 h). Tests on uncoated Ti-6-2-4-2 indicated the stress to produce 0.2% plastic strain at 922 K is very low, of the order of 7 MN/m^2 (1 ksi) (Table 8).

Because of the relatively poor performance of the alloys and coatings in the hot-salt stress-corrosion test, coated Ti-6-2-4-2 specimens and potential coating alloys were not tested under stressed conditions in this test. Instead, their effectiveness in resisting oxygen contamination was evaluated from coupons exposed for 3.6×10^5 s (100 h) at 922 K (1200°F) in Task A. In the cases where the scale is reasonably pore-free, and of uniform thickness, the extent of oxygen contamination can be inferred from a comparison of the measured weight gain with the calculated oxygen content of the observed oxide film, after making certain assumptions concerning its density. In cases where the scale morphology precludes accurate measurement of its thickness, microhardness traverses over the thickness of the sectioned alloy provide a good qualitative assessment of the extent of oxygen

TABLE 14. LONGITUDINAL CREEP AND TENSILE PROPERTIES OF Ti-6Al-2Sn-4Zr-2Mo WITH TITANIUM ALUMINIDE COATINGS

Specimen Number	Coating Type	Surface Condition	755 K (900°F) Creep Exposure Data						Room Temperature Tensile Test Data						
			Time		Stress		Plastic Strain, %		UTS		YS		El., %	RA, %	
			sec	hrs	MN/m²	ksi			MN/m²	ksi	MN/m²	ksi			
4	Al/TiAl$_3$	As dipped	No Exposure						979	142	862	125	15	28	
14	Al/TiAl$_3$	As dipped	3.6 x 10^5	100	172	25	0.199		1096	159	972	141	16	27	
3	Al/TiAl$_3$	Salt	3.6 x 10^3	1 *	172	25	--		--	--	--	--	--	--	
19	Al/TiAl$_3$	Salt	1.38 x 10^5	38.2*	138	20	--		--	--	--	--	--	--	
20	Al/TiAl$_3$	Salt	9.9 x 10^4	27.5*	103	15	--		--	--	--	--	--	--	
8	TiAl	As dipped, annealed(a)	No Exposure						972	141	827	120	13	22	
24	As received, annealed(a)	Bare	No Exposure						972	141	841	122	15	25	
15	TiAl	As dipped, annealed	3.6 x 10^5	100	172	25	0.134		1089	158	924	134	13	16	
25	As received, annealed	Bare	3.6 x 10^5	100	172	25	0.097		1082	157	958	139	14	22	
11	TiAl	Salt	3.96 x 10^3	1.1*	172	25	--		--	--	--	--	--	--	
13	TiAl	Salt	1.15 x 10^4	3.2*	138	20	--		--	--	--	--	--	--	
17	TiAl	Salt	1.32 x 10^5	36.6*	103	15	--		--	--	--	--	--	--	
6	TiAl	Salt	2.02 x 10^4	5.6*	69	10	--		--	--	--	--	--	--	
23	As received, annealed	Salt	3.49 x 10^4	9.7*	172	25	--		--	--	--	--	--	--	
22	Ditto	Salt	3.6 x 10^5	100	103	15	0.093		986	143	965	140	2	7	

(a) 2.23 x 10^5 s (62 h) at 922 K (1200 F) followed by 8.64 x 10^4 s (24 h) at 1089 K (1500 F).

* Failed in creep test under the load and at the exposure time indicated.

TABLE 15. SUMMARY OF MICROHARDNESS MEASUREMENTS OF Ti ALLOYS
(Microhardness values in Vickers Hardness (Hv)
numbers)

Alloy	Unoxidized (as cast)		Oxidized		Distance*, μm
	Center	Edge	Center	Edge	
Ti	112 ± 3	107 ± 3	116 ± 3	345 ± 10 to 596 ± 25	265
Ti-6Al-2Sn-4Zr-2Mo**	296 ± 8	326 ± 9	312 ± 9	596 ± 25	450
Ti-55Ni	236 ± 11	236 ± 11	233 ± 11	585 ± 24	up to 75
Ti-63Al (TiAl$_3$)	473 ± 17	473 ± 17	503 ± 19	483 ± 18	--
Ti-35Al (TiAl)	350 ± 10	420 ± 15	290 ± 7	275 ± 7	--
Ti-16Al (Ti$_3$Al)	353 ± 10	353 ± 10	346 ± 10	312 ± 8	--
Ti-8Cr-15Al	578 ± 23	578 ± 23	502 ± 19	476 ± 17	--
Ti-15Cr-15Al	600 ± 25	574 ± 25	607 ± 25	585 ± 25	--
Ti-25Cr-8Al	514 ± 20	563 ± 20	585 ± 25	590 ± 25	--
Nb-42Ti-9Cr-6.5Al	364 ± 11	364 ± 11	408 ± 14	577 ± 23	40
Nb-40Ti-9Cr-4Al	415 ± 13	398 ± 13	377 ± 13	638 ± 27	50
Nb-42Ti-4Cr-4Al**	310 ± 9	310 ± 9	295 ± 8	476 ± 17	40 to 65

*   Depth from edge over which hardness has been increased.

**   Rolled sheet.

contamination. The results of such microhardness measurements made using
an attachment on a Reichert MeF metallograph at 100 g load, are compared
in Table 15. In addition to rating the alloys for resistance to oxygen
ingress, these data also provide a useful comment on the suitability of
the alloys for use as coatings, assuming that it is reasonable to equate
the hardness of these castings to the ductility expected in coatings made
from the same alloys. In particular it appears that the hardness of the
titanium aluminide increases in the order Ti-35Al $\leq$ Ti-16Al $<$ Ti-63Al, and that
the hardness of the Ti-16Al alloy is progressively increased by additions
of chromium.

CONCLUSIONS

- Titanium aluminides can provide good barriers to oxygen
  ingress as measured by weight gain kinetics in oxidation
  tests for 3.6×10^5 s (100 h) at 922 K (1200°F), and by
  an assessment of hardening resulting from interstitial
  oxygen and nitrogen uptake of the alloys during this test.
  The relatively low ductility of these alloys, however,
  might limit their usefulness as coatings.

- Only the Ti-63Al alloy derived oxidation resistance from the
  formation of an alumina scale, the Ti-35Al and Ti-16Al alloys
  formed modified TiO_2 scales. Chromium additions did not
  increase the oxidation resistance of Ti-16Al, but effected
  marked changes in the oxide scale morphology, possible
  through a hardening effect on the alloy matrix.

- The Ti-35Al and Ti-16Al intermetallics are subject to hot-
  salt stress-corrosion cracking at 755 K (900°F). Both
  suffer preferential corrosion of an aligned phase in this
  test which possibly results in the formation of notches.

- Protective, alumina scales can be formed on Nb-Cr-Al-base
  alloys, but these alloys are extremely brittle in bulk form.

- Ductile, β-type Nb-Ti-Cr-Al alloys can offer resistance to
  oxygen ingress almost equivalent to that of Ti-16Al, but these
  alloys form modified TiO_2, not alumina, scales.

- A ductile Nb-40Ti-4Cr-4Al alloy suffered embrittlement in the
  HSSC test at 755 K, but the embrittlement appeared to be
  largely the result of oxygen contamination rather than salt
  attack.

- A ductile Ti-55Ni alloy exhibited limited resistance to oxygen contamination at 922 K (1200°F), but was little affected by exposure in a HSSC test at 755 K (900°F).

- Coatings of Si, Al/Cr, Al/Cr/Mg, Al/TiAl$_3$ and TiAl on Ti-6-2-4-2 did not provide protection in a HSSC test at 755 K. The susceptibility to this test was in some cases increased, apparently as a result of cracks occurring in the brittle coatings and propagating into the alloy matrix.

- The effectiveness of electrochemical suppression of the HSSC reaction was not evaluated. The techniques used in this program were unable to introduce the desired electrochemically-active elements into a coating on Ti-6-2-4-2.

SUGGESTIONS FOR FUTURE WORK

The concept of barrier layer coatings having some inherent ductility appears to have some merit for the environmental protection of titanium alloys at high temperatures. The ductile barrier layer alloys tested were not greatly susceptible to hot-salt cracking, but failed in the HSSC test largely as a result of oxygen/nitrogen embrittlement. Modification of these alloys to increase their resistance to oxygen penetration should be investigated as a route to viable barrier layer systems. Ti-35Al might also find application as a barrier layer alloy (of limited ductility) if its HSSC threshold stress can be increased by the elimination of interphase corrosion through the use of a single-phase alloy.

Since most coating systems designed for high-temperature oxidation resistance can protect Ti-6-2-4-2 from oxygen contamination, the concept of a duplex coating comprising an inner ductile barrier layer with an outer, oxidation-resistant layer might also be considered.

ACKNOWLEDGEMENTS

BIBLIOGRAPHY

(1) H. R. Gray, "Hot-Salt Stress-Corrosion of Titanium Alloys as Related to Turbine Engine Operation", NASA TMS-68015, May 1972.

(2) M. T. Groves, "Environmental Protection to 922 K (1200°F) for Titanium Alloys", NASA CR-134537, November 1973.

(3) M. Garfinkle, "An Electrochemical Model for Hot-Salt Stress-Corrosion of Titanium Alloys", NASA TN D-6779, April 1972, and Met. Trans. 4 1677 (1973).

(4) D. L. Deadmore, "Cyclic Oxidation of Co-Cr-Al-Y and Aluminide Coatings on IN-100 and VIA Alloys in High-Velocity Gases", NASA TN D-6842, July, 1972.

(5) M. A. Gedwill and S. J. Grisaffe, "Oxidation Resistant Claddings for Superalloys", NASA TM X-67925, October 1971.

(6) D. V. Ignatov, Z. I. Kornilova, and E. Lazarev, "Structural and Kinetic Investigations Into Oxidizibility of Titanium and Its Alloys, and Their Protection Against High-Temperature Gas Corrosion", in Titanium Science and Technology, Vol 4, 1973, R. I. Jaffee and H. M. Burte, eds.

(7) I. A. Zelenkov and E. N. Martynchuk, "Heat Resistance of Titanium Aluminide-Niobium Alloys at 800-1000°C", Akad, Nauk, Ukrain. SSR, Metallofizika, 1972 (42), 66.

(8) C. T. Sims, W. D. Klopp, and R. I. Jaffee, Trans. Am. Soc. Metals, 51, 256 (1959).

(9) E. M. Lazarev, et al, "The Oxidation of Nb-Ti-Al Alloys at High Temperatures", Zhur. Priklad. Khim, 46 (1), 48 (1973).

(10) D. J. Maykuth, et al, "Development of Corrosion-Resistant Niobium-Base Alloys", Report No. BMI-1437 on AEC Contract No. W-7405-eng-92 (1960).

(11) T. N. Rhodin, U.S. Patent No. 2,838,396, assigned to E. I. DuPont de Nemours & Co. (1958)

(12) J. Klein and A. G. Metcalfe, "Tungsten Fiber Reinforced Oxidation Resistant Columbium Alloys", Final Report by Solar to Naval Air Systems Command on Contract No. N00019-71-C-0158 (1972).

(13) R. I. Jaffee, F. R. Schwartzberg, and D. N. Williams, "Columbium-Titanium Base Oxidation-Resistant Alloys", U.S. Patent No. 2,940,845 assigned to Kennecott Copper Corp. (1960).

(14) L. Kaufman and H. Nesor, "Computer Analysis of Alloy Systems", AFML-TR-73-56, March 1973.

(15) T. T. Nartova and G. G. Sopochkin, "Study of Phase Equilibrium of Alloys of the Ti-Al-Nb Ternary System", Novyy Konstruksionny Material-Titan, 1972, pp 19-23 (Transl. FTD-HT-23-120-74).

(16) V. G. Gromova and A. M. Grishanova, "Properties of Stable Titanium-Niobium Based β-Alloys", ibid, pp 118-120 (Transl. FTD-HT-23-140-74).

(17) N. M. Fedorchuk, D. V. Ignatov, and V. G. Gromova, "Oxidizability of AN-Type β-Alloys of Titanium and Protecting Them Against Gas Corrosion", ibid, pp 135-138 (Transl. FTD-HT-23-144-74).

(18) N. M. Fedorchuk, D. V. Ignatov, and L. A. Petrova, "Oxidizability of the IVTI Titanium β-Alloy and its Protection From Gas Corrosion", ibid, pp 131-134 (Transl. FTD-HT-23-144-74).

(19) B. A. Stein, H. B. Dexter, and D. M. Royster, "Coatings and Surface Treatments for Longtime Protection of Ti-8Al-Mo-1V Alloy Sheet From Hot-Salt Stress Corrosion", NASA TN D4319, March, 1968.

(20) E. L. Kochka and V. C. Peterson, "The Salt Corrosion of Titanium Alloys at Elevated Temperatures", Final Tech. Rept., Contract No. NOas 60-6004-C, Crucible Steel Co., January 1961.

(21) V. C. Peterson and H. B. Bomberger, "The Mechanism of Salt Attack on Titanium Alloys", ASTM Spec. Publ. No. 397, 1966.

(22) J. F. Nejedlik, "Development of Improved Coatings for Ni- and Co-Base Alloys", Tech. Rept. AFML-TR-70-208, December, 1970.

(23) North American Rockwell, work on NASA Contract NAS7-200, December 1971.

(24) G. J. Hermeil, D. N. Braski, D. M. Royster, and H. B. Dexter, "Salt Stress Corrosion of Ti-8Al-1Mo-1V Alloy Sheet at Elevated Temperatures", ASTM Spec. Tech. Publ. No. 397, 1966.

(25) L. C. Covington and F. R. Early, "Methods of Protecting Titanium Against Hot-Salt Stress Corrosion", Progress Report No. 21, Titanium Metals Corp., August, 1964.

(26) R. A. Wood, "Surface Treatment of Titanium", DMIC Tech. Note, March 1965.

(27) F.J.J. van Loo and G. D. Rieck, "Diffusion in the Titanium-Aluminum System", Acta. Met., 21, 61 (1973).

(28) Private communication, E. S. Bartlett, Battelle's Columbus Laboratories.

APPENDIX A

DISTRIBUTION LIST FOR SUMMARY REPORT

A-1

DISTRIBUTION LIST FOR NASA CR-134661

CONTRACT NAS3-17761

(THE NUMBER IN PARENTHESIS SHOWS HOW MANY COPIES
IF MORE THAN ONE ARE TO BE SENT TO AN ADDRESS.)

MR. J. ACURIO
    MS 77-5
NASA LEWIS RESEARCH CTR.
21000 BROOKPARK ROAD
CLEVELAND, OHIO 44135

DR. R.L. ASHBROOK
    MS 49-3
NASA LEWIS RESEARCH CTR.
21000 BROOKPARK ROAD
CLEVELAND, OHIO 44135

MR. G.M. AULT
    MS 3-5
NASA LEWIS RESEARCH CTR
21000 BROOKPARK ROAD
CLEVELAND, OHIO 44135

MR. J.C. FRECHE
    MS 49-1
NASA LEWIS RESEARCH CTR
21000 BROOKPARK ROAD
CLEVELAND, OHIO 44135

DR. H.R. GRAY
    MS 49-1
NASA LEWIS RESEARCH CTR.
21000 BROOKPARK ROAD
CLEVELAND, OHIO 44135

MR. S.J. GRISAFFE
    MS 49-3
NASA LEWIS RESEARCH CTR
21000 BROOKPARK ROAD
CLEVELAND, OHIO 44135

MISS T.D. GULKO
    MS 49-3
NASA LEWIS RESEARCH CTR.
21000 BROOKPARK ROAD
CLEVELAND, OHIO 44135

MR. R.W. HALL
    MS 49-1
NASA LEWIS RESEARCH CTR
21000 BROOKPARK ROAD
CLEVELAND, OHIO 44135

MR. F.H. HARF   (20)
    MS 49-3
NASA LEWIS RESEARCH CTR
21000 BROOKPARK ROAD
CLEVELAND, OHIO 44135

MR. C.E. LOWELL
    MS 49-3
NASA LEWIS RESEARCH CTR.
21000 BROOKPARK ROAD
CLEVELAND, OHIO 44135

DR. G.J. SANTORO
    MS 49-3
NASA LEWIS RESEARCH CTR.
21000 BROOKPARK ROAD
CLEVELAND, OHIO 44135

MR. N.T. SAUNDERS
    MS 105-1
NASA LEWIS RESEARCH CTR
21000 BROOKPARK ROAD
CLEVELAND, OHIO 44135

DR. I. ZAPLATYNSKY
    MS 49-3
NASA LEWIS RESEARCH CTR.
21000 BROOKPARK ROAD
CLEVELAND, OHIO 44135

CONTRACTS SECTION B
    MS 500-313
NASA LEWIS RESEARCH CTR
21000 BROOKPARK ROAD
CLEVELAND, OH 44135

LIBRARY   (2)
            MS 60-3
   NASA LEWIS RESEARCH CTR
   21000 BROOKPARK ROAD
   CLEVELAND, OHIO 44135

REPORT CONTROL OFFICE
            MS 5-5
   NASA LEWIS RESEARCH CTR
   21000 BROOKPARK ROAD
   CLEVELAND, OHIO 44135

MAJ. H.L. STAUBS
   AFSC LIAISON MS 501-3
   NASA LEWIS RESEARCH CTR
   21000 BROOKPARK ROAD
   CLEVELAND, OHIO 44135

MR G. C. DEUTSCH / RW
   NASA HEADQUARTERS
   WASHINGTON, DC
                    20546

MR. N. REKOS / RL
   NASA HEADQUARTERS
   WASHINGTON, DC
                    20546

LIBRARY   MS 185
   NASA
   LANGLEY RESEARCH CENTER
   LANGLEY FIELD, VA 23365

LIBRARY
   NASA
   MARSHALL SPACE FLIGHT
   CENTER
   HUNTSVILLE, AL 35812

LIBRARY - ACQUISITIONS
   JET PROPULSION LAB.
   4800 OAK GROVE DRIVE
   PASADENA, CA 91102

PATENT COUNSEL
            MS 500-113
   NASA LEWIS RESEARCH CTR
   21000 BROOKPARK ROAD
   CLEVELAND, OHIO 44135

TECHNOLOGY UTILIZATION
            MS 3-19
   NASA LEWIS RESEARCH CTR
   21000 BROOKPARK ROAD
   CLEVELAND, OHIO 44135

LT.COL. G.J. WEDEN
   AMRDL   MS 77-5
   NASA LEWIS RESEARCH CTR.
   21000 BROOKPARK RD.
   CLEVELAND OH 44135

MR. J. GANGLER / RWM
   NASA HEADQUARTERS
   WASHINGTON, DC
                    20546

LIBRARY
   NASA
   GODDARD SPACE FLIGHT CTR
   GREENBELT, MARYLAND 20771

MR. J.G. WILLIAMSON
   NASA   S&E ASTN-MMC
   MARSHALL SPACE FLIGHT
   CENTER
   HUNTSVILLE, AL 35812

TECHNICAL LIBRARY / JM6
   NASA
   MANNED SPACECRAFT CENTER
   HOUSTON, TX 77058

LIBRARY
   NASA FLIGHT RESEARCH CTR
   P.O. BOX 273
   EDWARDS, CALIFORNIA 93523

LIBRARY - REPORTS
      MS 202-3
  NASA AMES RESEARCH CENTER
MOFFETT FIELD, CA 94035

DEFENCE DOCUMENTATION CTR
 CAMERON STATION
 5010 DUKE STREET
ALEXANDRIA, VIRGINIA
           22314

MR. J.J. CROSBY
  AFML/LLP
  HEADQUARTERS
  WRIGHT PATTERSON AFB,
        OH   45433

MR. N. GEYER
  AFML/LLP
  HEADQUARTERS
  WRIGHT PATTERSON AFB,
      · OH   45433

MR. J.R. WILLIAMSON
  AFML/LT
  HEADQUARTERS
  WRIGHT PATTERSON AFB,
        OH   45433

MR. R. SCHMIDT AIR-52031A
  NAVAL AIR SYSTEMS COMMAND
  NAVY DEPARTMENT
  WASHINGTON, DC   20361

DR. C.W. SPENCER
  MATERIALS ADV. BD.
  NAT. ACAD. OF SCIENCES
  2101 CONSTITUTION AVE.
  WASHINGTON, DC   20418

MR. H.E. BOYER
  AM. SOCIETY FOR METALS
  METALS PARK
  NOVELTY, OH 44073

ACQUISITIONS BRANCH (10)
  NASA SCIENTIFIC & TECHN.
  INFORMATION FACILITY
  BOX 33
  COLLEGE PARK, MD 20740

MR. M. SLAWSKY
  USAF OFF SCIENTIFIC RES
  PROPULSION RESEARCH DIV
  WASHINGTON, DC   20525

MR. J. PENTER
  AFML/LLM
  HEADQUARTERS
  WRIGHT PATTERSON AFB
        OH   45433

DR. J.S. MYERS
  AFIT/DE
  HEADQUARTERS
  WRIGHT PATTERSON AFB.
        OH 45433

MR. M. LEVY   AMXMR-RM
  ARMY MATERIALS AND
  MECHANICS RESEARCH CTR.
  WATERTOWN, MA   02172

TECHNICAL REPORTS LIBRARY
  OAK RIDGE NATIONAL LAB.
  OAK RIDGE, TENN. 37830

DR. P.G. SHEWMON
  DIR. DIV. OF MTLS. RES.
  NAT. SCIENCE FOUNDATION
  WASHINGTON, DC 20550

DR. N.A. TINER
  INSTIT. OF SURFACE TECHN.
  CALIFORNIA STATE COLLEGE
  LONG BEACH, CALIFORNIA
            90801

LIBRARY
UNIVERSITY OF DAYTON
RESEARCH INSTITUTE
300 COLLEGE PARK AVE
DAYTON, OHIO 45409

MR. G.B. BARTHOLD
ALUMINUM CO. OF AMERICA
1200 RING BLDG
WASHINGTON, DC 20036

MR. W.E. BINZ
BOEING COMPANY
P.O. BOX 3733
SEATTLE, WA 98124

MR. M. NEGRIN
CHROMALLOY CORP.
169 WESTERN HIGHWAY
WEST NYACK, NEW YORK
10994

DR. R.F. KIRBY
GARRETT AIRESEARCH
DEPT. 93-393
402 S. 36TH STREET
PHOENIX, AR 85034

LIBRARY
CRD
GENERAL ELECTRIC COMPANY
P.O. BOX 8
SCHENECTADY, N.Y. 12301

DR. I.I. BESSEN
AEG/GED
GENERAL ELECTRIC COMPANY
CINCINNATI, OHIO 45215

DR. M. HERMAN
DETROIT DIESEL AILISON DV
P.O. BOX 894
INDIANAPOLIS, IN 46206

REPORTS ACQUISITION
AEROSPACE CORPORATION
P.C. BOX 95085
LOS ANGELES, CALIFORNIA
90045

MR. S. GOLDBLATT
AVCO LYCOMING DIV.
550 S. MAIN STREET
STRATFORD, CT 06497

LIBRARY
CHRYSLER CORPORATION
DEFENSE-SPACE GROUP
P.C. BOX 757
DETROIT, MI 48231

MR. J.R. GUERNSEY
COLT INDUSTRIES
CRUCIBLE INC.
P.C. BOX 88
PITTSBURGH, PA. 15230

MR. R.K. MALIK
CONVAIR AEROSPACE DIV.
GENERAL DYNAMICS CORP.
P.C. BOX 80847
SAN DIEGO, CA 92138

LIBRARY
ADVANCED TECHNOLOGY LAB
GENERAL ELECTRIC COMPANY
SCHENECTADY, NY 12345

MR. T.K. REDDEN
AEG/GED
GENERAL ELECTRIC COMPANY
CINCINNATI, OHIO 45215

MR. D.S. NICHOLS PT.8 T2B
DETROIT DIESEL ALLISON DV
P.C. BOX 894
INDIANAPOLIS, IN 46206

MR. L.C. MCCANDLESS
GENERAL TECHNOLOGIES CORP
1821 M.FARADAY DRIVE
RESTON, VIRGINIA 22070

MR. A. STELSON
SOLAR DIVISION
INTERNATIONAL HARVESTER
2200 PACIFIC HIGHWAY
SAN DIEGO, CAL. 92112

MR.R. PERKINS
LOCKHLED PALO ALTO R.LAB.
3251 HANOVER STREET
PALO ALTO,CA 94304

DR. J.W. BOND
DIRECTOR OF RESEARCH
PHYSICS TECHNOLOGY LABS.
7841 EL CAJON BOULEVARD
LA MESA, CALIFORNIA 92041

DR. H.B. BOMBERGER
DIRECTOR OF RESEARCH
REACTIVE METALS CORP
NILES, OHIO 44446

DR. J.C. WILLIAMS
ROCKWELL INTERNATIONAL
SCIENCE CENTER
THOUSAND OAKS, CALIFORNIA
91360

DR. R. BECK
TELEDYNE-CAE
1330 LASKEY ROAD
TOLEDO, OH 43601

MR. R. BROADWELL
TITANIUM METALS CORP.
WEST CALDWELL, NJ 07006

MR. F. BOTT
INSULATION SYSTEMS INC.
11233 CONDOR AVENUE
FOUNTAIN VALLEY, CALIF.
92703

DR. J. BERKOWITZ
ARTHUR D. LITTLE,INC.
20 ACORN PARK
CAMBRIDGE, MASSACHUSETTS
02140

MR. D.L. KUMMER
MCDONNELL DOUGLASS ASTR.
MCDONNELL DOUGLAS CORP.
P.O. BOX 516
ST. LOUIS, MO 63166

MR. G.J. WILE
POLYMET CORPORATION
10597 CHESTER ROAD
CINCINNATI, OH 42515

MR. H.D. KESSLER
REACTIVE METALS INC.
100 WARREN AVENUE
NILES,OHIO 44446

MR.L. SAMA
SYLVANIA ELEC.PROD.,INC.
CHEM. AND MET.DIV.
CANTIAGUE ROAD
HICKSVILLE NY 11802

MR. E. WAKEFIELD   MS144
TEXAS INSTRUMENTS INC.
P.C. BOX 5936
DALLAS TX 75222

DR. J. GADD
TRW INC
1400 N.CAMERON ST
HARRISBURG, PENNSYLVANIA
17105

MR. J.A. ALEXANDER
  MATERIALS TECHNOLOGY
  TRW EQUIPMENT GROUP
  23555 EUCLID AVENUE
  CLEVELAND, OHIO 44117

LIBRARY
  MATERIALS TECHNOLOGY
  TRW EQUIPMENT GROUP
  23555 EUCLID AVENUE
  CLEVELAND, OH 44117

RESEARCH LIBRARY
  UNITED AIRCRAFT CORP.
  400 MAIN STREET
  EAST HARTFORD,   CT
                     06105

MR. E. GREKILA
  WESTINGHOUSE RESEARCH LAB
  BEULAH ROAD
  CHURCHILL, PENNSYLVANIA
                     15535

DR. M.T. GROVES
  MATERIALS TECHNOLOGY
  TRW EQUIPMENT GROUP
  23555 EUCLID AVENUE
  CLEVELAND, OHIO 44117

DR. R.C. TUCKER, JR
  MATERIALS SYSTEMS DIV.
  UNION CARBIDE CORPORATION
  P.C. BOX 24184
  INDIANAPOLIS IN   46224

MR. R.G. SHERMAN
  DIRECTOR OF ENGINEERING
  VALLEY-TODECO INC
  SYLMAR, CALIFORNIA 91342